

1 **Bering Sea surface water conditions during Marine**  
2 **Isotope Stages 12 to 10 at Navarin Canyon (IODP Site**  
3 **U1345)**

4  
5 **Beth E. Caissie<sup>1</sup>, Julie Brigham-Grette<sup>2</sup>, Mea S. Cook<sup>3</sup>, Elena Colmenero-**  
6 **Hidalgo<sup>4</sup>**

7 [1]{Iowa State University, Ames, Iowa}

8 [2]{University of Massachusetts, Amherst, Amherst, Massachusetts}

9 [3]{Williams College, Williamstown, Massachusetts}

10 [4]{Universidad de León, León, Spain}

11 Correspondence to: B.E. Caissie ([bethc@iastate.edu](mailto:bethc@iastate.edu))

12

13 **Abstract**

14 Records of past warm periods are essential for understanding interglacial climate system  
15 dynamics. Marine Isotope Stage 11 occurred 425-394 ka when global ice volume was the  
16 lowest, sea level was the highest and terrestrial temperatures were the warmest of the last  
17 500 kyrs. Because of its extreme character, this interval has been considered an analog  
18 for the next century of climate change. The Bering Sea is ideally situated to record how  
19 opening or closing of the Pacific-Arctic Ocean gateway (Bering Strait) impacted primary  
20 productivity, sea ice, and sediment transport in the past; however, little is known about  
21 this region prior to 125 ka. IODP Expedition 323 to the Bering Sea offered the  
22 unparalleled opportunity to look in detail at time periods older than had been previously  
23 retrieved using gravity and piston cores. Here we present a multi-proxy record for Marine  
24 Isotope Stages 12-10 from Site U1345 located near the continental shelf-slope break.  
25 MIS 11 is bracketed by highly productive laminated intervals that may have been  
26 triggered by flooding of the Beringian shelf. Although sea ice is reduced during the early  
27 MIS 11 laminations, it remains present at the site throughout both glacials and MIS 11.

28 High summer insolation is associated with higher productivity, but colder SSTs, which  
29 implies that productivity was likely driven by increased upwelling. Multiple examples of  
30 Pacific-Atlantic teleconnections are presented including laminations deposited at the end  
31 of MIS 11 in sync with brief expansions in sea ice in the Bering Sea and stadial events  
32 seen in the North Atlantic. When global eustatic sea level was at its peak, an series of  
33 anomalous conditions are seen at U1345. We examine whether this is evidence for a  
34 reversal of Bering Strait Through Flow, an advance of Beringian tidewater glaciers, or a  
35 turbidite.

36

## 37 **1 Introduction**

38 Predictions and modeling of future climate change require a detailed understanding of  
39 how the climate system works. Reconstructions of previous warm intervals shed light on  
40 interhemispheric teleconnections. The most recent interglacial period with orbital  
41 conditions similar to today was approximately 400 ka, during the extremely long  
42 interglacial known as Marine Isotope Stage (MIS) 11. CO<sub>2</sub> concentration averaged  
43 approximately 275 ppm, which is similar to pre-industrial levels (EPICA Community  
44 Members, 2004). The transition from MIS 12 into MIS 11 has been compared to the last  
45 deglaciation (Dickson et al., 2009) and extreme warmth during MIS 11 has been  
46 considered an analog for future warmth (Droxler et al., 2003; Loutre and Berger, 2003),  
47 although the natural course of interglacial warmth today has been disrupted by  
48 anthropogenic forcing (IPCC, 2013).

49 Despite the work done to characterize the warmth of MIS 11 in the terrestrial realm  
50 (Candy et al., 2014; Melles et al., 2012; Prokopenko et al., 2010), as well as the North  
51 Atlantic (Bauch et al., 2000; Chaisson et al., 2002; Dickson et al., 2009; Milker et al.,  
52 2013; Poli et al., 2010), little is known about this interval from the North Pacific and  
53 Bering Sea region (Candy et al., 2014). Modeling studies describe several mechanisms  
54 for linking the Atlantic and Pacific through oceanic heat transport on glacial-interglacial  
55 time scales (DeBoer and Nof, 2004; Hu et al., 2010), however, there have been no tests of  
56 these modeling studies using proxy data older than 30 ka. Furthermore, the location of the  
57 Bering Sea marginal sea ice zone advanced and retreated hundreds of kilometers during

58 the past three glacial-interglacial cycles (Caissie et al., 2010; Katsuki and Takahashi,  
59 2005; Sancetta and Robinson, 1983); however, sea surface and intermediate water  
60 variability before MIS 5 is unknown.

61 This investigation of terrestrial-marine coupling at the shelf-slope break from MIS 12 to  
62 10 is the first study of this interval in the subarctic Pacific (Fig. 1). We use a multi-proxy  
63 approach to examine orbital- and millennial-scale changes in productivity and sea ice  
64 extent. We demonstrate that insolation plays a major role in these changes, but that sea  
65 ice also shows rapid, millennial-scale variability. Finally, we test the hypotheses that 1) in  
66 Beringia, tidewater glaciers advanced while sea level was high and 2) Bering Strait  
67 Through Flow reversed shortly after the MIS 12 glacial termination (Termination V). We  
68 find inconclusive evidence of a glacial advance, but no evidence of Bering Strait reversal.

69

## 70 **2 Background**

### 71 **2.1 Global and Beringian Sea Level during MIS 11**

72 The maximum height of sea level during MIS 11 is an open question with estimates  
73 ranging from 6 to 13 m above present sea level (apsl) (Dutton et al., 2015) to 0 m apsl  
74 (Rohling et al., 2010; Rohling et al., 2014). The discrepancy may stem from large  
75 differences between global eustatic (Bowen, 2010) or ice-volume averages (McManus et  
76 al., 2003) and regional geomorphological or micropaleontological evidence (van  
77 Hengstum et al., 2009). Regional isostatic adjustment due to glacial loading and  
78 unloading are now known to be significant and regional highstands may record higher  
79 than expected sea levels if glacial isostasy and dynamic topography have not been  
80 accounted for, even in places that were never glaciated (PAGES et al., 2016; Raymo and  
81 Mitrovica, 2012; Raymo et al., 2011). For example, Raymo and Mitrovica (2012) suggest  
82 eustatic sea level during MIS 11 was 6-13 m apsl globally and near 5 m apsl locally in  
83 Beringia, yet MIS 11 shorelines are at +22 m today in northwest Alaska (Kaufman and  
84 Brigham-Grette, 1993) due to this complex geophysics.

85 Regardless of the ultimate height of sea level, the transition from MIS 12 to MIS 11  
86 records the greatest change in sea level of the last 500 ka (Rohling et al., 2014); sea level

87 rose from perhaps -140 m to its present level or higher (Bowen, 2010)(Dutton et al.,  
88 2015). Sea level during MIS 11 may have been complex (Kindler and Hearty, 2000), but  
89 most records agree that sea level during this exceptionally long interglacial (30 kyrs) was  
90 highest from 410 to 401 ka, coincident with a second peak in June insolation at 65°N.  
91 This long highstand most likely requires partial or complete collapse of the Greenland ice  
92 sheet (up to 6 m) (de Vernal and Hillaire-Marcel, 2008; Reyes et al., 2014) and/or the  
93 West Antarctic Ice Sheet (Scherer et al., 1998), but not the East Antarctic Ice Sheet  
94 (Berger et al., 2015; Dutton et al., 2015; Raymo and Mitrovica, 2012). It has frequently  
95 been hypothesized that the West Antarctic Ice Sheet collapsed during MIS 11 and  
96 modeling studies confirm this (Pollard and DeConto, 2009), however unconformities in  
97 the record prevent confirmation of a collapse (McKay et al., 2012). Yet, Teitler (2015)  
98 show that IRD during MIS 11 dropped as low as it was during MIS 31, when it is clear  
99 that the West Antarctic Ice Sheet had collapsed (Naish et al., 2009). With uncertainties,  
100 East Antarctica ice was stable; however, small changes in either sector of the Antarctic  
101 ice sheet may have contributed up to 5 m of sea level rise (Berger et al., 2015; EPICA  
102 Community Members, 2004).

103 The sea level history of Beringia defines Arctic communication between the Pacific and  
104 the Atlantic oceans during the Plio-Pleistocene. As a region, Beringia consists of both the  
105 terrestrial and marine regions north of the Aleutian Islands that stretch to the shelf-slope  
106 break in the Bering, East Siberian, Chukchi, and Beaufort seas (Fig. 1). On land, Beringia  
107 extends from the Lena River in Siberia to the Mackenzie River in Canada. Large portions  
108 of the Beringian shelf were exposed when sea level dropped below -50 m (Hopkins,  
109 1959) and this subaerial expanse stretches more than 1000 km from north to south during  
110 most glacial periods (Fig. 2). In contrast, as sea level rises at glacial terminations the  
111 expansive continental shelf is flooded, rapidly once sea level reaches -60 mapsl (Keigwin  
112 et al., 2006). This introduces fresh organic matter and nutrients into the southern Bering  
113 Sea (i.e. Bertrand et al., 2000; Shiga and Koizumi, 2000; Ternois et al., 2001), re-  
114 establishing at -50 mapsl the connection between the Pacific and Atlantic oceans through  
115 Bering Strait (Keigwin et al., 2006). The late Cenozoic history of the depth of the Bering  
116 Strait sill is poorly known, hence current oceanographic reconstructions (e.g., Knudson  
117 and Ravelo, 2015) assume that a sill depth of -50 mapsl was temporally stable, which is

118 probably not the case and requires future study. However, in this study, we also assume  
119 that a sill depth of -50 maps<sub>l</sub> controls oceanographic communication between the Atlantic  
120 and Pacific Oceans.

121

## 122 **2.2 Site Location and Oceanographic Setting**

123 The Integrated Ocean Drilling Program's (IODP) Expedition 323, Site U1345, is located  
124 on an interfluvial ridge near the shelf-slope break in the Bering Sea (Fig. 1). Navarin  
125 Canyon, one of the largest submarine canyons in the world (Normack and Carlson, 2003)  
126 is located just to the northwest of the site. Sediments were retrieved from ~1008 m of  
127 water, placing the site within the center of the modern day oxygen minimum zone  
128 (Takahashi et al., 2011). We focus on this site because of its proximity to the modern  
129 marginal ice zone in the Bering Sea and observed high sedimentation rates. Its siting on  
130 top of an interfluvial ridge was chosen to reduce the influence of turbidites moving through  
131 Navarin Canyon.

132 Today, water circulates cyclonically in the deep basins of the Bering Sea (Fig. 1). Site  
133 U1345 is influenced by the northwest flowing Bering Slope Current (BSC), which is  
134 derived from the Alaskan Stream (AS). South of the Aleutian Islands, the Alaskan  
135 Stream flows westward and enters the Bering Sea through deep channels in the western  
136 Aleutian Islands. Once north of the Aleutian Islands, this water mass becomes the  
137 Aleutian North Slope Current (ANS), and flows eastward until it reaches the Bering Sea  
138 shelf. Interactions with the shelf turn this current to the northwest where it becomes the  
139 Bering Slope Current (Stabeno et al., 1999). Tidal forces and eddies in the Bering Slope  
140 Current drive upwelling through Navarin Canyon and other interfluvial ridges along the shelf-  
141 slope break (Kowalik, 1999). The resulting cold water and nutrients brought to the sea  
142 surface, coupled with the presence of seasonal sea ice, drive the high productivity found  
143 today in the so called "Green Belt" (Springer et al., 1996) along the shelf-slope break.  
144 North of the site, low salinity, high nutrient shelf waters (Cooper et al., 1997) primarily  
145 flow north through the Bering Strait to the Arctic Basin (Schumacher and Stabeno, 1998).

146

## 147 **3 Methods**

### 148 **3.1 Age Model**

149 The age model (Fig. 3) is derived from the shipboard age model, which was developed  
150 using magnetostratigraphy and biostratigraphy. First and last appearance datums for  
151 diatoms and radiolarians make up the majority of the biostratigraphic markers used to  
152 place the record in the correct general stratigraphic position (Takahashi et al., 2011).  
153 Oxygen isotope measurements taken on the benthic foraminifera, *Uvigerina peregrina*,  
154 *Nonionella labradorica*, and *Globobulimina affinis* (Cook et al., 2016) were then used to  
155 tune site U1345 to the global marine benthic foraminiferal isotope stack (LR04) (Lisiecki  
156 and Raymo, 2005) (Fig. 3; Table 1). Based on this combined age model, MIS 11 spans  
157 from 115.3 to 130.6 mbsf (Cook et al., 2016); however, the characteristic interglacial  
158 isotopic depletion was not found in U1345 which means that the exact timing of peak  
159 interglacial conditions is unknown.

160 The nearby core, IODP Exp 323, Site U1343 (Fig. 1) has an excellent oxygen isotopic  
161 record during MIS 11 (Asahi et al., 2016). We compared the two isotopic records and  
162 their magnetic susceptibilities (Fig. 3) and found that even with only two tie points, there  
163 was good correlation between the timing of the onset of laminated intervals and also the  
164 interglacial increase in magnetic susceptibility (Fig. 3b). We added one additional tie  
165 point to connect the inflection points in magnetic susceptibility (Table 1). In U1343, this  
166 point occurred at 398.50 ka. U1345 was shifted 1.5 ka younger in order to align with  
167 U1343. The addition of this point allows us to have more confidence in the timing of  
168 peak interglacial conditions in U1345. However, given the oxygen isotope sampling  
169 resolution, as well as the stated error in the LR04 dataset (4 kyr), we estimate the error of  
170 the age model could be up to 5 kyr. Therefore, we urge caution when comparing  
171 millennial scale changes at this site with other sites that examine MIS 11 at millennial  
172 scale resolution or finer.

173 Sedimentation rates during the study interval range from 29 cm/kyrs to 45 cm/kyr with  
174 the highest sedimentation rates occurring during glacial periods. Depths and ages of  
175 major climate intervals referred to in the text are found in Table 2.

176

## 177 **3.2 Sediment Analyses**

178 Details about sediment sampling can be found in the Supplementary Materials.  
179 Quantative diatom slides were prepared (Scherer) and counted (Schrader and Gersonde,  
180 1978) using published taxonomic descriptions and images (Hasle and Heimdal, 1968;  
181 Koizumi, 1973; Lundholm and Hasle, 2008, 2010; Medlin and Hasle, 1990; Medlin and  
182 Priddle, 1990; Onodera and Takahashi, 2007; Sancetta, 1982, 1987; Syvertsen, 1979;  
183 Tomas, 1996; Witkowski et al., 2000). Diatom taxa were then grouped according to  
184 ecological niche (Table 3) based on biological observations (Aizawa et al., 2005; Fryxell  
185 and Hasle, 1972; Håkansson, 2002; Horner, 1985; Saito and Taniguchi, 1978;  
186 Schandelmeier and Alexander, 1981; von Quillfeldt, 2001; von Quillfeldt et al., 2003)  
187 and statistical associations (Barron et al., 2009; Caissie et al., 2010; Hay et al., 2007;  
188 Katsuki and Takahashi, 2005; Lopes et al., 2006; McQuoid and Hobson, 2001; Sancetta,  
189 1982, 1981; Sancetta and Robinson, 1983; Sancetta and Silvestri, 1986; Shiga and  
190 Koizumi, 2000). In cases where a diatom species was reported to fit into more than one  
191 environmental niche, it was grouped into the niche where it was most commonly  
192 recognized in the literature.

193 Eighteen quantitative calcareous nannofossil slides were prepared (Flores and Sierro,  
194 1997) and counted using a Zeiss polarized light microscope at 1000x magnification.  
195 Samples were considered barren if no coccoliths were found in at least 165 randomly  
196 selected fields of view. All taxa were identified to the species or variety level (Flores et  
197 al., 1999; Young et al., 2003).

198 Grain size of both biogenic and terrigenous sediment was measured using a Malvern  
199 Mastersizer 3000 with the Hydro MV automated wet dispersion unit. The mineralogy of  
200 ten samples was analyzed using a Siemens D-5000 X-Ray Diffractometer (Eberl, 2003)

201 The carbon and nitrogen isotopic and elemental composition of organic matter was  
202 determined by Dumas combustion using a Carlo Erba 1108 elemental analyzer coupled to  
203 a Thermo-Finnigan Delta Plus XP isotope ratio mass spectrometer at the University of  
204 California Santa Cruz Stable Isotope Laboratory. The 1-sigma precision of stable isotope  
205 measurements and elemental composition of carbon are 0.2‰ and 0.03%, respectively,  
206 and for nitrogen are 0.2‰ and 0.002%, respectively.  $\delta^{13}\text{C}$  values are reported relative to

207 the Vienna Pee Dee Belemnite (VPDB) and  $\delta^{15}\text{N}$  values are reported relative to  
208 atmospheric  $\text{N}_2$ . Percent  $\text{CaCO}_3$  was calculated according to Schubert and Calvert (2001).  
209 More detailed methodology can be found in the Supplemental Materials.

210

## 211 **4 Results**

### 212 **4.1 Sedimentology**

213 The sediments at Site U1345 are massive with centimeter-scale dark or coarse-grained  
214 mottles. They are mainly composed of clay and silt with varying amounts of diatoms,  
215 sand, and tephra throughout. Laminated intervals bracket MIS 11 (Fig. 4). The proportion  
216 of diatoms relative to terrigenous or volcanogenic grains is highest during laminated  
217 intervals and lowest immediately preceding Termination V (~425 ka). Vesiculated tephra  
218 shards were seen in every diatom slide analyzed. Several thin (< 1 cm) sand layers and  
219 shell fragments were visible on the split cores, especially during MIS 12. However, high-  
220 resolution grain size analyses show that the median grain size was lowest during MIS 12,  
221 increasing from approximately 14  $\mu\text{m}$  to 21  $\mu\text{m}$  at the start of Termination V at 424.5 ka  
222 (130.92 mbsf). Median grain size peaks at 84  $\mu\text{m}$  between 401 and 407 ka (125.42-  
223 123.62 mbsf). This interval is also the location of an obvious sandy layer in the core.  
224 After this “anomalous interval,” median grain size remains steady at about 17  $\mu\text{m}$ .  
225 Subrounded to rounded clasts (granule to pebble) commonly occur on the split surface of  
226 the cores. We combined clast and sand layer data from all Holes at Site U1345 when  
227 examining their distribution (Fig. 4).

228 A 3.5 m thick laminated interval, estimated to span 12 kyrs (see Table 4 for depths and  
229 ages) is deposited beginning during Termination V. Although the termination is short-  
230 lived and the laminated interval quite long, we refer to it as the Termination V  
231 Laminations for the sake of clarity throughout this manuscript. The next laminated  
232 interval occurs at about 394 ka and lasts approximately 1.1 kyrs. During the transition  
233 from late MIS 11 to MIS 10, a series of four thin laminated intervals are observed. Each  
234 interval lasts between 0.34 and 1.25 ka (Table 4). In general, the upper and lower  
235 boundaries of laminated intervals are gradational; however the boundaries between  
236 individual lamina are sharp (Takahashi et al., 2011). There are two types of laminations.



237 The Termination V Laminations are Type I laminations: millimeter-scale alternations of  
238 black, olive gray, and light brown triplets. In addition to containing a high proportion of  
239 diatoms, this type of laminated interval also contains high relative proportions of  
240 calcareous nannofossils and foraminifera (Takahashi et al., 2011). The majority of  
241 laminations are parallel; however, a 7 cm interval during the Termination V Laminations  
242 is highly disturbed in Hole A, showing recumbent folds in the laminations (Takahashi et  
243 al., 2011). This interval was not sampled. Type II laminations occur throughout the  
244 remainder of MIS 11. These laminations have fewer diatoms and tend to be couplets of  
245 siliciclastic sediments with <40% diatoms (Takahashi et al., 2011). Percent CaCO<sub>3</sub> also  
246 increases during these laminations though foraminifera and calcareous nannofossils are  
247 very rarely seen. None of these later laminated intervals contain any evidence of  
248 disturbance.

## 249 **4.2 Mineralogy**

250 We determined the weight percent of 23 common minerals in ten samples across the  
251 study interval. Samples are primarily composed of quartz, plagioclase, tephra, illite and  
252 chlorite with minor amounts of other clay and non-clay minerals (Table 5). Downcore,  
253 the largest variability occurs in the weight percent of quartz, chlorite, and illite. In  
254 general, chlorite comprises nearly 35% of the minerals present in the sediments until 408  
255 ka, and then declines ~ 5% for the remainder of MIS 11. Conversely, quartz increases  
256 from 425 to 406 ka and then comprises ~15% of the minerals for the remainder of MIS  
257 11. Illite is lower than 2% of the mineral assemblage at 424 ka, and then increases rapidly  
258 to nearly 10% at 422 ka. It remains near 10% for the remainder of MIS 11 except for a  
259 brief negative excursion at 406 ka.

260

## 261 **4.3 Diatoms**

### 262 **4.3.1 Diatom Assemblages**

263 A total of 97 different diatom taxa were identified. Individual samples include between  
264 26 and 46 taxa each with an average of 37 taxa. Both types of laminated intervals contain  
265 fewer taxa than bioturbated intervals do. This decrease in diversity is confirmed using the

266 Margalef, Simpson, and Shannon indices (Maurer and McGill, 2011) which all show  
267 similar down-core profiles (Fig. 5). The Margalef index is a measure of species richness.  
268 It shows a decrease in the number of taxa during four out of five laminated intervals that  
269 are sufficiently well sampled. Between laminated intervals, there is also a noted decrease  
270 in taxa at 388 ka. The Simpson index measures the evenness of the sample. Values close  
271 to 1 indicate that all taxa contain an equal number of individuals, while values close to 0  
272 indicate that one species dominates the assemblage. In general, the Simpson index is  
273 close to 1 throughout the core; however, during the Termination V Laminations and the  
274 most recent two laminations, the Simpson index decreases reflecting the dominance by  
275 *Chaetoceros* RS during these intervals (Fig. 5). The Simpson index never approaches 0,  
276 which would likely indicate a strong dissolution signal. The Shannon diversity index  
277 measures both species richness and evenness. Correspondingly, it is low during three of  
278 the laminated intervals, high during MIS 12 and peaks at 397 ka (Fig. 5).

279 Absolute diatom abundances vary between  $10^6$  and  $10^8$  diatoms deposited per gram of  
280 sediment with values an order of magnitude higher during most laminated intervals than  
281 during massive intervals (Fig. 5). The diatom assemblage is dominated by *Chaetoceros*  
282 and *Thalassiosira antarctica* resting spores (RS), with lesser contributions from  
283 *Fragilariopsis oceanica*, *Fragilariopsis cylindrus*, *Fossula arctica*, *Shionodiscus trifultus*  
284 (= *Thalassiosira trifulta*), *Thalassiosira binata*, small (<10  $\mu\text{m}$  in diameter) *Thalassiosira*  
285 species, *Paralia sulcata*, *Lindavia* cf. *ocellata*, *Neodenticula seminae*, and *Thalassionema*  
286 *nitzschioides* (Fig. 6).

287

#### 288 **4.3.2 Qualitative Diatom Proxies**

289 Diatoms, like many organisms, thrive m

290 under a specific range of environmental conditions or optima and these optima are  
291 different for each species. For this reason, diatom assemblages are excellent  
292 paleoceanographic indicators (Smol, 2002). We grouped diatoms with similar  
293 environmental niches together (Table 3) to interpret the paleoceanographic sea surface  
294 conditions at the Bering Sea shelf-slope break during MIS 12 to 10 (Caissie, 2012;  
295 Katsuki and Takahashi, 2005; Sancetta, 1982){Caissie and Nesterovich, In Prep} (Fig. 7).

296 Grouping diverse species together may result in a loss of information when two different  
297 species in the same niche show differing abundance patterns over time. On the other  
298 hand, changes in abundances may simply reflect different species filling the same niche  
299 at different times.

300 *Chaetoceros* resting spores are the dominant taxa included in the high productivity group  
301 (Table 3). Relative percent abundances of *Chaetoceros* RS are highest (up to 69%) during  
302 the Termination V Laminations and follow the pattern of both diatom accumulation rate  
303 and insolation at 65° N (Berger and Loutre, 1991). The lowest relative abundances (15-  
304 20%) of *Chaetoceros*/high productivity species occur between 403 and 390 ka (124.21 to  
305 120.07 mbsf) when both obliquity and insolation are low (Fig. 7h).

306 Epontic diatoms are those that bloom attached to the underside of sea ice or within brine  
307 channels in the ice (Alexander and Chapman, 1981). This initial bloom occurs below the  
308 ice as soon as enough light penetrates to initiate photosynthesis in the Bering Sea, which  
309 can occur as early as March (Alexander and Chapman, 1981). A second ice-associated  
310 bloom occurs as sea ice begins to break up on the Bering Sea shelf. This bloom is  
311 referred to as the marginal ice zone bloom and many of its members are common species  
312 in the sediment assemblage. Several diatom species are present in both types of sea ice  
313 blooms, and so while they are indicators of ice presence, they cannot be used to  
314 distinguish between types of sea ice. These species are grouped under “both ice types”  
315 (Table 3).

316 Epontic species are present in low relative percent abundances (< 5%) throughout much  
317 of the record, but there is a marked absence of them during the laminated interval from  
318 423 to 410 ka (129.96-126.45 mbsf) (Fig. 7i). Marginal ice zone species fluctuate  
319 between 4% and 14% throughout the record and do not show any trends in abundance  
320 changes (Fig. 7j). The grouping of species found both within the ice and in the water  
321 surrounding ice, however, is also somewhat reduced during laminated intervals (Fig. 7k).

322 A cold layer of water found between seasonally warmer surface and warmer deep water  
323 characterizes dicothermal water. It is stable because of its very low salinity. In the Sea of  
324 Okhotsk and the Bering Sea today, the dicothermal layer is associated with melting sea  
325 ice. Genera present in the Bering Sea during late summer tend to co-vary with the

326 dicothermal water indicators, so the two groups were merged for comparison with other  
327 diatom groups. *S. trifultus* is the dominant species in the dicothermal group (Table 3). It  
328 is relatively high (~4%) during MIS 12, is virtually absent from the sediments during the  
329 Termination V Laminations, and then increases again until it peaks at 10% relative  
330 abundance at 400 ka (123.22 mbsf) (Fig. 6).

331 Neritic species maintain ~10% relative abundance throughout the core (Fig. 7m). The  
332 dominant species in the neritic group is *Paralia sulcata* (Table 3), sometimes considered  
333 an indicator of shallow, moving water (Sancetta, 1982). Neritic species are lowest during  
334 the Termination V Laminations and increase dramatically around 404 ka (124.61 mbsf)  
335 to almost 50% of the assemblage (Fig. 7n). *L. cf. ocellata* is the dominant taxa in the  
336 fresh water group. This group is notably absent from much of the core, but prevalent  
337 between 401 and 392 ka (123.70 mbsf and 121.20 mbsf); it reaches its highest relative  
338 percent abundance (12%) at 401 ka (123.62 mbsf) (Fig. 7n).

339 *Neodenticula seminae* is used here as a tracer of Pacific water (Caissie et al., 2010;  
340 Katsuki and Takahashi, 2005). Absolute abundances begin to increase at 422 ka as global  
341 eustatic sea level rises above -50 mapsl. Abundance then decreases slowly over the  
342 course of the Termination V Laminations and peaks again at 392 ka and 382 ka. As sea  
343 level drops below -50 mapsl, *N. seminae* is no longer present at U1345. Relative percent  
344 abundances remain stable at ~2% relative percent abundance between 422 and 400 ka  
345 (129.62-123.62 mbsf), then peak at 13% at 392 ka (121.22 mbsf) (Fig. 6 and 7o).

346 Diatoms associated with warmer water or classified as members of temperate to  
347 subtropical assemblages (Table 3) are quite low throughout the record (<5%), and are  
348 highest (3-4%) during mid to late MIS 11 approximately ~410 to 391 ka (126.74 to  
349 116.50 mbsf) (Fig. 7p).

350

#### 351 **4.4 Calcareous Nannofossils**

352 Calcareous nannofossils were examined between 432-405 ka (133.4 to 125.0 mbsf); one  
353 third of the samples were barren (Fig. 7g, open purple circles) and only one sample (418  
354 ka; 128.8 mbsf) had sufficient individuals to estimate relative percent abundances (Fig.

355 7g). This sample is located midway through the Termination V Laminations when the  
356 diatom assemblage is overwhelmingly dominated by *Chaetoceros* RS. Small  
357 *Gephyrocapsa* dominates (>50%) the calcareous nannofossil assemblage. There are 35%  
358 medium *Gephyrocapsa*, 9% *Coccolithus pelagicus*, and 1% *Gephyrocapsa oceanica*.

359

## 360 **4.5 Geochemistry**

### 361 **4.5.1 Organic and Inorganic Carbon Content**

362 Total organic carbon (TOC) roughly follows the trend of relative percent abundances of  
363 *Chaetoceros* RS, with higher values during the Termination V Laminations (Fig. 7b, 7h).  
364 Mean TOC value during MIS 12 is 0.76%, and during the Termination V Laminations, it  
365 is 1.11%. TOC decreases between 408 (125.82 mbsf) and 404 ka (124.77 mbsf) coeval  
366 with a decrease in  $\delta^{15}\text{N}$  values. After 404 ka, it increases linearly to 374 ka (115.39  
367 mbsf). TOC is again high during the late MIS 11/MIS 10 laminations.

368 In contrast, inorganic carbon, calculated as %  $\text{CaCO}_3$  is less than 1% for most of the  
369 record (Fig. 7g). However, it increases up to 3.5% during the laminated intervals and also  
370 at 382 ka (117.87 mbsf), 392 ka (110.00 mbsf), and 408 ka (125.82 mbsf).

371

### 372 **4.5.2 Terrigenous vs. Marine Input Indicators**

373 Nitrogen, carbon and their isotopes can be used to determine relative amounts of  
374 terrigenous vs. marine organic matter input. Total nitrogen (TN) is significantly correlated  
375 with total organic carbon (TOC) (Fig. 8a); however, the y-intercept of a regression line  
376 through the data is 0.03 (Fig. 8a), indicating that there is a significant fraction of  
377 inorganic nitrogen in the sediments (Schubert and Calvert, 2001). Inorganic nitrogen can  
378 be adsorbed onto clay particles or incorporated into the crystal lattice of potassium-rich  
379 clays such as illite. This complicates interpretations of elemental nitrogen and its isotopes  
380 because the presence of inorganic nitrogen will lower  $\text{C}_{\text{org}}/\text{N}$  ratios and  $\delta^{15}\text{N}$  values  
381 (Muller, 1977; Schubert and Calvert, 2001).

382 Bearing this bias in mind, the relative terrigenous contribution to the sediments can be  
383 estimated by examining where U1345 samples plot in relation to typical  $\text{C}_{\text{org}}/\text{N}$ ,  $\delta^{15}\text{N}$ , and

384  $\delta^{13}\text{C}$  values for marine phytoplankton, refractory soil organic matter, and C3 vascular  
385 plants (Fig. 8). Note that we use  $\text{N}/\text{C}_{\text{org}}$ , the inverse of  $\text{C}_{\text{org}}/\text{N}$ , because we seek to derive  
386 the terrigenous carbon fraction rather than the fraction of terrigenous nitrogen (Perdue  
387 and Koprivnjak, 2007). Throughout MIS 12-10, organic matter is comprised of a mixture  
388 of marine and terrigenous organic matter. There is a higher contribution of marine  
389 organic matter during MIS 12, 10, and between 394 and 405 ka and a higher contribution  
390 of terrigenous organic matter during peak MIS 11 (Fig. 8). The  $\text{N}/\text{C}_{\text{org}}$  ratio indicates that  
391 during peak MIS 11, this terrigenous organic matter is likely refractory soil organic  
392 matter, rather than fresh vascular plant organic matter (Fig. 8b).

393 During MIS 12,  $\text{C}_{\text{org}}/\text{N}$  is highly variable, when sea level is below -50 m apsl (Fig. 7). As  
394 sea level rises during Termination V,  $\text{C}_{\text{org}}/\text{N}$  values increase from 6 to more than 9. The  
395 highest  $\text{C}_{\text{org}}/\text{N}$  value occurs at the start of the Termination V Laminations.  $\text{C}_{\text{org}}/\text{N}$   
396 decreases as sea level rises until at 400 ka (123.62 mbsf) it stabilizes near 7 for the  
397 remainder of the record (Fig. 7).

398 Carbon isotopic values range between -22 ‰ and -26 ‰. No sample has low enough  $\delta^{13}\text{C}$   
399 values to be comprised fully of typical Arctic Ocean marine phytoplankton (-22 to -19‰)  
400 or ice-related plankton (-18.3‰) (Schubert and Calvert, 2001); however samples from  
401 MIS 10, MIS 12, and the “anomalous interval” all plot close to marine phytoplankton  
402 values (Fig. 8b). At the onset of the Termination V Laminations,  $\delta^{13}\text{C}$  becomes more  
403 negative and then gradually increases to a maximum of -22.33 at 404 ka (124.62). After  
404 400 ka (123.5 mbsf),  $\delta^{13}\text{C}$  is relatively stable around -23.5‰ (Fig 7).

405

### 406 **4.5.3 Nitrogen Isotopes**

407 The nitrogen isotopic composition of bulk marine sediments can be thought of as a  
408 combination of the  $\delta^{15}\text{N}$  of the source nitrate and the amount of nitrogen utilization by  
409 phytoplankton (Brunelle et al., 2007). Denitrification is common in the low oxygen  
410 waters of the eastern tropical North Pacific (Liu et al., 2005) and in the Bering Sea during  
411 the Bølling-Allerød (Schlung et al., 2013), leading to enriched core top  $\delta^{15}\text{N}$  values  
412 between 8 and 9‰. When diatoms utilize nitrogen, they preferentially assimilate the  
413 lighter isotope,  $^{14}\text{N}$ , which enriches surface waters with respect to  $^{15}\text{N}$  (Sigman et al.,

414 1999). Complete nitrogen utilization would result in  $\delta^{15}\text{N}$  values identical to that of the  
415 source nitrate (Sigman et al., 1999). Sponge spicules (very low  $\delta^{15}\text{N}$  values) and  
416 radiolarians (highly variable  $\delta^{15}\text{N}$  values) may contaminate the  $\delta^{15}\text{N}$  of bulk organic  
417 matter; therefore, we looked for and found no correlation between spicule abundance and  
418  $\delta^{15}\text{N}$  in our samples.

419  $\delta^{15}\text{N}$  is relatively stable, but quite high throughout the study interval, fluctuating around  
420 an average value of 6.4‰ and reaching values greater than 7‰ and up to 8‰ several  
421 times (Fig. 7). There are several notable excursions from these high values. Coeval with  
422 sea level rise and increased relative percent *Chaetoceros* RS,  $\delta^{15}\text{N}$  decreased 2.7‰ to  
423 4.4‰ before recovering to average values during the Termination V Laminations. Two  
424 other depletions occur at 405 ka (124.77 mbsf) and 393 ka (121.62 mbsf), the first is the  
425 most extreme and reaches 2.9‰.

426

## 427 **5 Discussion**

### 428 **5.1 Orbital-Scale Changes in Productivity and Sea Ice**

429 The observed changes in diatom assemblages and lithology (Fig. 7) allow us to break the  
430 sedimentary record into five zones: MIS 12, Termination V, Peak MIS 11, Beringian  
431 Glacial Initiation, and Late MIS 11 (Table 2). These zones reflect changing sea ice,  
432 glacial ice, sea level, and SST and correspond to events recognized elsewhere in ice cores  
433 and marine and lake sediments.

434

#### 435 **5.1.1 Marine Isotope Stage 12 and Early Deglaciation (431-425 ka)**

436 From 431 to 425 ka, the record chronicles conditions at the end of MIS 12. Although  
437 diatom accumulation rate is quite low, a relatively diverse assemblage characterizes this  
438 period (Fig. 5) with moderate amounts of sea ice, high productivity, and dicothermal  
439 species (Fig. 7), indicating seasonal sea ice with highly stratified waters during the ice-  
440 melt season. Nitrogen isotopes indicate high nutrient utilization (Fig. 7) consistent with  
441 nitrogen-limited productivity in stratified waters as well as localized denitrification.  
442 Numerous shell fragments, two sand layers and the highest percentages of clay-sized

443 sediments in the record were deposited during MIS 12 (Figs 4 and 8) indicating input of  
444 terrigenous material, however, crossplots of elemental ( $C_{org}/N$  or  $N/C_{org}$ ) and isotopic  
445 ( $\delta^{13}C$ ,  $\delta^{15}N$ ) indicators of terrigenous and marine carbon pools indicate that the organic  
446 matter during MIS 12 is a diverse mix of marine phytoplankton and soil detritus (Fig. 8)  
447 likely derived from in-situ, but low, productivity and transport by several methods  
448 including large, oligotrophic rivers and downslope transport. Glacial ice was likely  
449 restricted to mountain-valley glaciers, similar to the last glacial maximum (e.g.  
450 Glushkova, 2001). These small, distant glaciers would not have produced large amounts  
451 of ice bergs though occasional glacial ice rafted debris (IRD) may have come from the  
452 Koryak Mountains, the Aleutians or Beringia. Consistent with this, sediments typical of  
453 glacial IRD, such as dropstones, are sparse, but present. In addition, sea ice rafting tends  
454 to preferentially entrain clay and silt (Reimnitz et al., 1998) and is likely to be an  
455 important contributor of terrigenous sediments.

456

#### 457 **5.1.2 Termination V (425-423 ka)**

458 Termination V is the transition from MIS 12 to MIS 11. Worldwide, it is a rapid  
459 deglaciation that is followed by a long (up to 30 kyrs) climate optimum (Milker et al.,  
460 2013). At U1345, gradually increasing productivity coupled with decreasing nutrient  
461 utilization and sea ice occurs between 425 and 423 ka. This is seen as an increase in  
462 absolute diatom abundances and relative percent abundance of *Chaetoceros* RS and a  
463 decrease in sea ice diatoms and  $\delta^{15}N$  values (Fig. 7). It is plausible that increased nitrogen  
464 availability drove higher primary productivity as floods scoured fresh organic matter  
465 from the submerging continental shelf (Bertrand et al., 2000). Rapid input of bioavailable  
466 nitrogen as the shelf was inundated has been suggested to explain increasing productivity  
467 during the last deglaciation in the Sea of Okhotsk (Shiga and Koizumi, 2000) and during  
468 MIS 11 in the North Atlantic (Poli et al., 2010) and also may have contributed to dysoxia  
469 by ramping up nutrient recycling, bacterial respiration, and decomposition of organic  
470 matter in the Bering Sea.

471



### 472 **5.1.3 Peak MIS 11 (423-394 ka)**

473 Globally, peak interglacial conditions (often referred to as MIS 11.3 or 11c) are centered  
474 around 400 to 410 ka (Dutton et al., 2015; Raymo and Mitrovica, 2012), though the exact  
475 interval of the temperature optimum varies globally and lasted anywhere from 10 to 30  
476 kyrs (Kandiano et al., 2012; Kariya et al., 2010; Milker et al., 2013). At U1345, peak  
477 interglacial conditions begin during the Termination V Laminations at 423 ka and  
478 continue until 394 ka, lasting nearly 30 kyrs consistent with the synthesis of the PAGES  
479 Past Interglacials working group (2016).

480

#### 481 **5.1.3.1 Laminations (423-410 ka)**

482 A 3.5 m thick laminated interval is deposited during early MIS 11 beginning at 423 ka  
483 (Fig. 7) when insolation was high at 65°N (Berger and Loutre, 1991). Its presence  
484 indicates that the bottom water at 1,000 m in the Bering Sea was dysoxic for more than  
485 11 kyrs. These laminations are characterized as Type I laminations with a high diatom  
486 content (Fig. 4). Several lines of evidence point towards high productivity among  
487 multiple phytoplankton groups as opposed to simply a change in preservation. First, we  
488 see an increase in diatom abundances by two orders of magnitude increase since MIS 12,  
489 second, a low-diversity diatom assemblage dominated by *Chaetoceros* RS, third, an  
490 abrupt increase in percent organic carbon, and fourth, high percent CaCO<sub>3</sub> and abundant  
491 calcareous nannofossils dominated by small *Gephyrocapsa*. Furthermore, enriched  $\delta^{15}\text{N}$   
492 values indicate either increased nitrogen utilization that likely led to this increased  
493 productivity or localized denitrification in low oxygen waters (Fig. 7).

494 Sea ice extent is reduced during this interval with almost no eponitic diatoms present and  
495 reduced amounts of other sea ice diatoms (Fig. 7). Geochemical crossplots indicate a high  
496 contribution from soil detritus and C3 plant organic matter (Fig. 8). At the onset of the  
497 laminated interval (423 ka),  $\delta^{13}\text{C}$  decreases and C<sub>org</sub>/N increases rapidly (Fig. 7) as the  
498 tundra-covered Bering Sea shelf is flooded.

499 However, the diatom record during the laminated interval has the lowest contribution of  
500 neritic diatoms and virtually no fresh water diatoms (Fig. 7), suggesting that although

501 terrigenous organic matter was an important input at the site, coastal, river, or  
502 swamp/tundra diatoms were not carried out to U1345 with this terrigenous organic  
503 matter.

504

#### 505 **5.1.3.2 Post Laminations (410-394 ka)**

506 Both high  $N/C_{org}$  and  $\delta^{13}C$  indicate that input of terrigenous organic matter is highest at  
507 the onset of the Termination V Laminations and then declines until mid MIS 11 (400 ka)  
508 at which time the organic matter is largely derived from marine phytoplankton (Fig. 7;  
509 red to grey dots in Fig. 8). This may be related to rising eustatic sea level causing the  
510 migration of the paleoshoreline farther northward and away from U1345.

511 Throughout MIS 11, *Chaetoceros* RS, a species indicative of high productivity, is  
512 generally higher when insolation is higher and lower when insolation is lower (404-390  
513 ka; Fig. 7). However, although their fluctuations are small, warm water species show the  
514 opposite trend, with higher proportions of warm water diatoms when insolation is low  
515 (Fig. 7). If higher proportions of warm water diatoms indicate warmer water, then this  
516 suggests that productivity is highest in colder waters but when insolation is high, and  
517 lowest in warmer waters when insolation is low. This may reveal a relationship between  
518 upwelling of colder waters and high productivity.

519

#### 520 **5.1.4 Late MIS 11 to MIS 10 (younger than 394 ka)**

521 After 394 ka, diatom productivity indicators are the lowest in the record but linearly  
522 increase to the top of the record. This is in contrast to a slight increase in diatom  
523 abundance, which increases at 393 ka and then remains relatively stable into MIS 10. Sea  
524 ice indicators also remain relatively high from 392 to the top of the record and  
525 dicothermal species reflect moderately stratified waters. Warm water species decrease  
526 from 390 ka to the top of the record (Fig. 7). The sum of this evidence indicates that at  
527 the end of MIS 11, summers were warm and sea ice occurred seasonally, perhaps lasting  
528 a bit longer than at other times in the record.

529 Eustatic sea level decreased beginning about 402 ka (Rohling et al., 2010), but sea level  
530 remained high enough to allow *N. seminae* to reach the shelf slope break until about 380  
531 ka (Fig. 7).

532

## 533 **5.2 The Bering Sea in the Context of Regional and Global Variability**

534 Across the Bering Sea, sediments at sites near Bowers Ridge (Fig. 1) are dominated by  
535 opal during MIS 11 (Kanematsu et al., 2013); whereas, biogenic sediments at sites along  
536 the Bering Slope, including U1345, are diluted by sea ice transport of lithogenic  
537 sediments as well as down-slope sediment transport (Kanematsu et al., 2013). However,  
538 the rate of biogenic opal accumulation is comparable for all sites in the Bering Sea,  
539 despite differences in sedimentation rates (Kanematsu et al., 2013; Stroynowski et al.,  
540 2015). Opal content in the sediments varies on glacial/interglacial time scales with high  
541 productivity during interglacials. Indeed, the highest percent opal concentration of the  
542 past 1 Ma occurs during MIS 11 at the two slope sites, U1345 and U1343 (Kanematsu et  
543 al., 2013).

544 Biogenic opal increases during early MIS 11 at Sites U1343 and U1345 (Kanematsu et  
545 al., 2013). At U1345, it mimics the pattern of relative percent abundance of *Chaetoceros*  
546 RS, the most abundant productivity indicator (Fig. 9). Although diatom data from other  
547 cored sites is low resolution (1-4 samples during MIS 11) (Kato et al., 2016; Onodera et  
548 al., 2016; Stroynowski et al., 2015; Teraishi et al., 2016), it provides a snapshot of diatom  
549 assemblages during MIS 11. Sea ice diatoms contribute approximately 30% of the diatom  
550 assemblages at the two slope sites, U1345 (this study) and U1343 (Teraishi et al., 2016),  
551 between 10 and 20% of the assemblage at the eastern Bowers Ridge site (U1340)  
552 (Stroynowski et al., 2015), but less than 2% of the assemblage on the western flanks of  
553 Bowers Ridge (U1341) (Onodera et al., 2016). In the North Pacific (ODP Site 884), no  
554 sea ice diatoms are present during MIS 11 (Kato et al., 2016). Site U1341 contained an  
555 assemblage high in dicothermal indicators such as *Shionodiscus trifultus*, and  
556 *Actinocyclus curvatulus*, oceanic front indicators such as *Rhizosolenia hebetata*, and *N.*  
557 *seminae* (Onodera et al., 2016), while the North Pacific (Site 884) assemblage is  
558 dominated by dicothermal indicators during MIS 11 (Kato et al., 2016). Percent opal

559 declines at Bowers Ridge during early MIS 11 at the same time as it increases at the slope  
560 sites (Iwasaki et al., 2016) (Fig. 9) when sea ice is reduced and upwelling along the shelf-  
561 slope break is increased. This implies that the relationship between productivity and sea  
562 ice in the Bering Sea is perhaps more complex than the simple idea that sea ice inhibits  
563 productivity (Iwasaki et al., 2016; Kim et al., 2016). The region is strongly influenced by  
564 winter sea ice throughout MIS 11 with seasonal sea ice present farther south along the  
565 slope than today and also in the eastern Bering Sea. Highly stratified waters, perhaps due  
566 to the seasonal expansion and retreat of sea ice, extended across the entire basin and even  
567 into the North Pacific.

568 Local ventilation of North Pacific Intermediate Water decreased as Bering Strait opened  
569 during Termination V with the weakest ventilation occurring around 400 ka (Knudson  
570 and Ravelo, 2015). This is coeval with the highest relative percent abundances of  
571 dicothermal diatoms indicating highly stratified water (Fig. 9).

572

### 573 **5.2.1 Temperature and Aridity during MIS 11**

574 When sea level was low during glacial periods such as MIS 12 (Rohling et al., 2010),  
575 U1345 was proximal to the Beringian coast (Fig. 2). With the Bering land bridge  
576 exposed, the continent was relatively cold and arid (Glushkova, 2001). In western  
577 Beringia, Lake El'gygytgyn was perennially covered with ice, summer air temperatures  
578 were warming in sync with increasing insolation from 4 to 12° C, but annual precipitation  
579 was low (200-400 mm) (Vogel et al., 2013).

580 As sea level rose, and global ice volume reached the lowest amount for the past 500 kyrs  
581 (Lisiecki and Raymo, 2005), the generally continental temperatures in the Northern  
582 Hemisphere increased (D'Anjou et al., 2013; de Vernal and Hillaire-Marcel, 2008;  
583 Lozhkin and Anderson, 2013; Lyle et al., 2001; Melles et al., 2012; Pol, 2011;  
584 Prokopenko et al., 2010; Raynaud et al., 2005; Tarasov et al., 2011; Tzedakis, 2010;  
585 Vogel et al., 2013) with a northward expansion of boreal forests in Beringia (Kleinen et  
586 al., 2014). However, the marine realm does not reflect this warming as strongly. At  
587 U1345, the relative percent warm water species suggest that SSTs during peak MIS 11  
588 were only slightly warmer than during MIS 12. Indeed, MIS 11 is not the warmest

589 interglacial in most marine records (Candy et al., 2014), rather MIS 5e is the warmest  
590 many places (PAGES et al., 2016). This is especially evident in the Nordic Seas where  
591 MIS 11 SSTs were lower than Holocene values (Bauch et al., 2000). However, MIS 11 is  
592 unique because it was much longer than MIS 5e in all records (PAGES et al., 2016). One  
593 exception to this is the Arctic Ocean, which was warm enough during MIS 11 to imply  
594 increased Pacific water input through Bering Strait (Cronin et al., 2013).

595 With elevated sea level, peak MIS 11c was very humid in many places. In the Bering  
596 Sea, modeling studies estimate up to 50 mm more precipitation than today at 410 ka  
597 (Kleinen et al., 2014). The most humid, least continental period recorded in the sediments  
598 at Lake Baikal occurs from 420-405 ka (Prokopenko et al., 2010), and extremely high  
599 precipitation is recorded at Lake El'gygytgyn on the nearby Chukotka Peninsula from  
600 420-400 ka (Melles et al., 2012).

601

## 602 **5.2.2 Millennial-Scale Laminations and Changes in Sea Ice**

603 Globally, late MIS 11 is characterized as a series of warm and cold cycles (Candy et al.,  
604 2014; Voelker et al., 2010), though there is no agreement on the timing of these cycles.  
605 At Site U1345, laminations are deposited intermittently between 394 and 392 ka and  
606 again after 375 ka (Fig. 4) as the climate transitioned into MIS 10. These laminations are  
607 quite different from the Termination V Laminations due to their shorter duration and lack  
608 of obvious shift in terrigenous vs. marine carbon source. In addition, these Type II  
609 laminations have higher diatom abundances and CaCO<sub>3</sub>, but lack increased upwelling  
610 indicators. Primary production during these laminations is likely not driven by nutrient  
611 upwelling along the shelf-slope break. Instead, most of these laminations show an  
612 increase in sea ice diatoms and roughly correspond with millennial scale stadial events  
613 that occurred during late MIS 11 in the North Atlantic (Fig. 9) (Voelker et al., 2010) as  
614 well as carbonate peaks at Blake Ridge (Chaisson et al., 2002). This suggests  
615 teleconnections between the Bering Sea and the North Atlantic at this time and places an  
616 indirect constraint on the depth of the Bering Strait sill.

617 It is tantalizing to note that the laminations occur at a time when global sea level was  
618 fluctuating near the sill depth of Bering Strait (-50 m apsl) (Rohling et al., 2010) (see

619 grey line at -50 m on Fig. 9). When sea level fluctuates near this level, Bering Strait  
620 modulates widespread climate changes that see-saw between the Atlantic and Pacific  
621 regions on millennial-scale time frames (Hu et al., 2010). And when Bering Strait is  
622 closed, North Pacific Intermediate Water formation increases (Knudson and Ravelo,  
623 2015). Further study will elucidate these connections.

624 A “Younger Dryas-like” temperature reversal is seen midway through Termination V in  
625 the North Atlantic (Voelker et al., 2010), Antarctica (EPICA Community Members,  
626 2004) and at Lake El’gygytyn (Vogel et al., 2013), however there is no evidence for  
627 such an event in the Bering Sea.

628

### 629 **5.2.3 Anomalous Interval (405-394 ka)**

630 The interval between 405 and 394 ka contains a number of unusual characteristics.  
631 Diatom assemblages are similar to those found in nearshore sediments from the Anvillian  
632 Transgression 800 km northeast of U1345 in Kotzebue Sound (Fig. 1) (Pushkar et al.,  
633 1999). A large peak in neritic species occurs at 404 ka followed by the highest relative  
634 percentages of fresh water species at the site and a slight increase in sea ice diatoms from  
635 400 to 394 ka (Fig. 7, grey bar). Primary productivity was low during this interval with  
636 the highest  $\delta^{15}\text{N}$  values of MIS 11, likely indicating denitrification. However, two large  
637 depletions in  $\delta^{15}\text{N}$  bracket this interval and occur as *Chaetoceros* RS decrease in relative  
638 percent abundance (Fig. 10). The organic matter is primarily sourced from marine  
639 phytoplankton, similar to the organic matter found during the two glacial intervals and  
640 distinctly different from the organic matter found during the rest of peak MIS 11 (Fig. 8).  
641 Detailed grain size analysis shows a fining upward trend of clay sized grains as well as a  
642 broad increase in sand sized grains and in particular grains greater than 250  $\mu\text{m}$  (Fig. 10).  
643 All samples are poorly to very poorly sorted (See Supplemental Material). Shipboard data  
644 shows an increase in the presence of pebbles, several sand layers (Fig. 10), and a thick  
645 interval of silty sand (Takahashi et al., 2011) at 404 ka (Fig. 4). While the presence of  
646 coarse material implies a terrestrial source for the sediments during this interval, this  
647 terrestrial matter must have been largely devoid of organic matter. The sum of this  
648 evidence leads us to investigate further three different interpretations of the interval

649 highlighted in grey on Fig. 10: a reversal of flow through Bering Strait, a tidewater  
650 glacial advance, and a turbidite.

651

### 652 **5.2.3.1 Reversal of Bering Strait Through Flow**

653 As sea level rose after MIS 12, the connection between the Pacific and the Atlantic was  
654 reestablished via Bering Strait. De Boer and Nof (2004) suggest that under high sea level  
655 conditions, if freshwater is suddenly released into the North Atlantic, the Bering Strait  
656 might act as an “exhaust valve” allowing fresh water from the Arctic Basin and the North  
657 Atlantic to flow into the Arctic Ocean and then flow south through the Bering Strait, thus  
658 preventing a shut-down in thermohaline circulation (DeBoer and Nof, 2004).

659 On St. Lawrence Island (Fig. 1), evidence for Arctic mollusks entering the Gulf of  
660 Anadyr suggests that flow through Bering Strait was reversed at some point during the  
661 Middle Pleistocene (Hopkins, 1972). Unfortunately, this event is poorly dated.

662 If flow were reversed due to a meltwater event (DeBoer and Nof, 2004), we would expect  
663 a temporary reduction in North Atlantic Deep Water (NADW) formation and an increase  
664 in southerly winds from Antarctica (DeBoer and Nof, 2004). In the Bering Sea, we would  
665 expect to see an increase in common Arctic or Bering Strait diatom species and a  
666 decrease in North Pacific indicators. In addition, the clay minerals in the Arctic Ocean are  
667 overwhelmingly dominated by illite (Ortiz et al., 2012), which tends to adsorb large  
668 amounts of ammonium (Schubert and Calvert, 2001). So, if net flow were to the south,  
669 one might expect to find increased illite and decreased  $C_{org}/N$  and  $\delta^{15}N$  values.

670 Proxy evidence for NADW ventilation indicates that between 412 and 392 ka, NADW  
671 formation decreased for short periods (< 1 ka) (Poli et al., 2010). In contrast, AABW  
672 formation appears to have drastically slowed around 404 ka, suggesting a decrease in sea  
673 ice and winds from around Antarctica as the southern hemisphere warmed (Hall et al.,  
674 2001).

675 At U1345, diversity is highest around 400 ka, due to the multiple contributions of Arctic  
676 species (fresh water, shelf, coastal, sea ice) and common pelagic diatoms, while the North  
677 Pacific indicator, *N. seminae* maintains low relative abundances and does not change  
678 throughout this interval. No marked increase in illite is observed during this interval in

679 either U1345 or elsewhere on the Bering Slope (Kim et al., 2016) (Fig. 9). However,  
680 chlorite, which dominates North Pacific sediments (Ortiz et al., 2012) decreases at 407 ka  
681 (Fig. 9), suggesting a reduced Pacific influence.  $C_{org}/N$  values began decreasing linearly  
682 starting at 409 ka, productivity sharply decreases at 406 ka,  $\delta^{15}N$  values are the most  
683 depleted at 405 ka, just 1 kyr before a conspicuous peak in *P. sulcata*, a common diatom  
684 found in the Bering Strait. Because there is conflicting evidence of both northward and  
685 southward flow, we reject the hypothesis of reversed flow through Bering Strait during  
686 MIS 11.

687

### 688 **5.2.3.2 Glacial Advance**

689 At its maximum, the Nome River Glaciation is the most extensive glaciation in central  
690 Beringia and is dated to Middle Pleistocene. Although it has not been precisely dated, it  
691 is likely correlative with late MIS 11 or MIS 10 (Kaufman et al., 1991; Miller et al.,  
692 2009). Nome River glaciomarine sediments recording the onset of rapid tidewater glacial  
693 advance are found in places such as St. Lawrence Island (Gualtieri and Brigham-Grette,  
694 2001; Hopkins, 1972), the Pribilof Islands (Hopkins, 1966), the Alaska Arctic coastal  
695 plain (Kaufman and Brigham-Grette, 1993), Kotzebue (Huston et al., 1990), Nome  
696 (Kaufman, 1992), and Bristol Bay (Kaufman et al., 2001) (Fig. 1). At these sites glaciers  
697 advanced, in some cases more than 200 km, and reached tidewater while eustatic sea  
698 level was high (Huston et al., 1990).

699 Although global sea level was near its maximum, and much of the world was  
700 experiencing peak MIS 11 conditions (Candy et al., 2014), there is evidence that the high  
701 latitudes were already cooling. At 410 ka, insolation at 65° N began to decline (Berger  
702 and Loutre, 1991), and cooling began at 407 ka in Antarctica, expressed both isotopically  
703 and as an expansion of sea ice (Pol, 2011). Millennial scale cooling events were recorded  
704 at Lake Baikal (Prokopenko et al., 2010). By 405 ka, there was some evidence globally  
705 for ice sheet growth (Milker et al., 2013) as Lake Baikal began to shift towards a dryer,  
706 more continental climate (Prokopenko et al., 2010) and productivity declined at Lake  
707 El'gygytgyn (Melles et al., 2012).



708 Solar forcing coupled with a proximal moisture source, the flooded Beringian shelf,  
709 drove snow buildup (Brigham-Grette et al., 2001; Huston et al., 1990; Pushkar et al.,  
710 1999) and glacial advance from coastal mountain systems. Precipitation at Lake  
711 El'gygytyn, just west of the Bering Strait, was two to three times higher than today at  
712 405 ka (Melles et al., 2012). A similar "snow gun" hypothesis has been invoked for other  
713 high latitude glaciations (Miller and De Vernal, 1992); however, Beringia is uniquely  
714 situated. Once sea level began to drop, Beringia became more continental and arid  
715 (Prokopenko et al., 2010) and the moisture source for these glaciers was quickly cut off.

716 Subaerial and glaciofluvial deposits below the Nome River tills and correlative  
717 glaciations indicate that Beringian ice, especially from the western Brooks Range,  
718 advanced as the climate grew colder. Ice wedges and evidence of permafrost are common  
719 (Huston et al., 1990; Pushkar et al., 1999) in sand and gravel deposits later overridden by  
720 Nome River till.

721 If evidence of the Nome River glaciation in central Beringia was present at U1345, we  
722 might expect to see evidence of glacial ice rafting. Previous work has suggested that  
723 sediments deposited by icebergs should be poorly sorted and skew towards coarser  
724 sediments (Nürnberg et al., 1994). Sediments greater than 150  $\mu\text{m}$  are likely glacially ice  
725 rafted (St. John, 2008), however it is not possible to distinguish sediments deposited by  
726 glacial versus sea ice on grain size alone (St. John, 2008). Both types of ice commonly  
727 carry sand-sized or larger sediments (Nürnberg et al., 1994). Sea ice diatoms should not  
728 be found in glacial ice, instead, we would expect glacial ice to be either barren, or to  
729 carry fresh water diatoms from ice-scoured lake and pond sediments. At U1345, there is a  
730 brief coarse interval (405-402 ka) followed by deposition of fresh water diatoms until 394  
731 ka.

732 Although it is tempting to assign this to the Nome River Glaciation, there are too many  
733 unknowns including whether the coarse grains were transported by sea ice, glacial ice, or  
734 some other method. Further work is ongoing to look for the onset of the Nome River  
735 Glaciation in both MIS 11 and MIS 13 as well as to distinguish the transport mechanism  
736 for these quartz grains.

737

738 **5.2.3.3 Turbidite**

739 The location of Site U1345 on a high interfluvial was chosen to minimize the likelihood  
740 that sediments could have been transported and deposited here by turbidites or other  
741 down-slope currents, yet evidence for a turbidite during this interval is very strong.  
742 Although there is no evidence of slumping or distorted sediments, clear erosive surfaces,  
743 or any structures that would indicate a turbidite during the anomalous interval, there are  
744 folded laminations elsewhere in the sediment core (Takahashi et al., 2011). If this interval  
745 was a turbidite, we would expect an erosive surface, overlain by clasts and perhaps a  
746 coarse sand layer followed by a fining up sequence. We see intermittent sand layers and  
747 small pebbles coupled with a linear increase in the percent clay throughout the interval  
748 (Fig. 10). Sediments are poorly sorted throughout the interval, consistent with rapid  
749 turbidite deposition and the presence of neritic and fresh water diatoms suggest  
750 redeposition of these sediments offshore from shallow water. Sancetta and Robinson  
751 (1983) argue that benthic pennate species were transported out of shallow water by rivers  
752 and turbidity currents during glacial periods; however, they do not consider ice as a  
753 transport mechanism. In this study, we have considered most benthic pennate species as  
754 members of either the eponitic or both ice ecological niches (von Quillfeldt et al., 2003).  
755 However, it is striking that the pattern of benthic pennate species at U1345 is nearly  
756 identical to that of the fresh water species.

757 Although the evidence is strongest for a turbidite, it is unusual to find just one turbidite as  
758 we might expect a turbidity flow to exist in the same place for a prolonged period.  
759 Further investigation of this and other Bering Sea cores can elucidate how common  
760 intervals like this are along the slope and if there is temporal consistency between  
761 deposits. The presence of a turbidite may suggest that the age model for this core needs to  
762 be slightly revised; however, there is no evidence of an erosive surface, nor a clear  
763 indication that all of the material deposited during this interval is allochthonous. In  
764 addition, the presence of a turbidite does not change the overall orbital and millennial  
765 scale interpretations of this record. Therefore, we choose to keep the age model as is.

766

## 767 **6 Conclusions**

768 This study aimed to describe orbital- and millennial-scale changes in productivity and sea  
769 ice extent in the Bering Sea, specifically at the shelf-slope break Site U1345. We further  
770 tested two hypotheses: 1) in Beringia, tidewater glaciers advanced while sea level was  
771 high and 2) Bering Strait Through Flow reversed shortly after the MIS 12 glacial  
772 termination (Termination V).

773 The interval between MIS 12 and MIS 10 is marked by large changes in productivity but  
774 only minor changes in sea ice extent at Site U1345. Productivity changed in concert with  
775 changes in insolation and water temperature. During warmer periods, high stratification  
776 appears to have led to lowered productivity. Site U1345 sites in the present-day oxygen  
777 minimum zone, and the presence of laminations frequently throughout the core indicates  
778 that oxygen is low. Evidence of denitrification is prevalent for much of the record, likely  
779 due to dysoxic conditions.

780 During MIS 12, productivity was low and seasonal sea ice dominated the Bering Sea with  
781 highly stratified waters during the ice-melt season. At Termination V, diatom  
782 productivity increased by two orders of magnitude while nitrogen utilization decreased.  
783 At 423 ka, an 11 kyr long laminated interval began. This interval was highly productive  
784 for multiple phytoplankton groups. The surface waters were relatively unstratified, and  
785 sea ice, though still present, decreased. This period is marked by the highest terrigenous  
786 organic matter input of the record possibly due to scouring of the continental shelf as sea  
787 level rose. During peak and late MIS 11, SSTs appear to have been warm, but seasonal  
788 sea ice lasted longer. And at the end of MIS 11, sea ice increased as sea level declined.

789 Laminations at the end of MIS 11 correspond with millennial scale stadials seen in the N  
790 Atlantic. These deposits represent possible evidence of teleconnections between the  
791 Atlantic and the Pacific as eustatic sea level fluctuated near the Bering Strait sill depth.

792 Decreased NADW formation and species transport from the Arctic Ocean southward  
793 support a reversal of the Bering Strait Current at 405 ka; however, there is no evidence  
794 for the transport of Arctic Ocean clay minerals or oceanographic forcing related to an  
795 increase in winds in Antarctica. Therefore, there is inconclusive evidence for a reversal of  
796 the Bering Strait Current during MIS 11.

797 When global sea level was at its maximum, insolation dropped and Beringia began to  
798 cool in sync with other polar regions. Sediments deposited during the so called,  
799 “anomalous interval” may have been carried by tidewater glaciers bringing neritic species  
800 far off shore. This glacial advance is attributed to humid conditions in Beringia that  
801 allowed rapid glacial growth. Alternatively, this interval may be a turbidite which could  
802 shift the age model for this core and cause this section to be omitted from the  
803 paleoceanographic record.

804 Previous studies have referred to MIS 11 as an analog for the next century of climate  
805 change. Today sea ice barely reaches Site U1345 even in winter and does not reach any  
806 other Bering Sea or North Pacific sites (U1340, U1341, U1343 or ODP 884). In contrast,  
807 during MIS 11, sea ice diatoms are present throughout the entirety of MIS 11 at U1345  
808 and seasonal sea ice appears to have reached both slope sites and the eastern Bowers  
809 Ridge (Onodera et al., 2016; Stroynowski et al., 2015; Teraishi et al., 2016). However,  
810 evidence for a reduction of sea ice in the Arctic Ocean during MIS 11 (Cronin et al.,  
811 2013) implies that while winter sea ice was expanded in the Bering Sea compared to  
812 today, summer sea ice was likely reduced. Such a significant difference may indicate that  
813 MIS 11 is not an ideal analog for climate change over the next 100 years.

814 However, there are lessons to be learned from the paleo-record. When sea ice declined  
815 during early MIS 11, nutrients were upwelled from the deep Bering Sea and flooding of  
816 the land bridge further brought nutrients into the surface waters. This caused productivity  
817 to increase at Sites U1345 and U1343. However, at Bowers Ridge Site U1341,  
818 productivity declined at this time. The pattern of primary productivity across the Bering  
819 Sea underscores that understanding the myriad drivers of primary productivity is essential  
820 as we prepared for decreased sea ice in the future.

821 Data used in this manuscript are archived at the National Center for Environmental  
822 Information (<https://www.ncei.noaa.gov>; specific doi and web address pending).

823

## 824 **Acknowledgements**

825 The authors thank the captain and crew of the JOIDES Resolution and Exp. 323 co-chief  
826 scientists Christina Ravelo and Kozo Takahashi. We acknowledge the two reviewers,  
827 Thomas Cronin and Jason Addison who provided us with thoughtful comments that  
828 greatly improved this manuscript. This work was partially supported by National Science  
829 Foundation, Office of Polar Programs Arctic Natural Sciences Award #1023537 and a  
830 Post Expedition Award from the Consortium for Ocean Leadership.

831 **References**

- 832 Aizawa, C., Tanimoto, M., and Jordan, R. W.: Living diatom assemblages from North  
833 Pacific and Bering Sea surface waters during summer 1999, *Deep-Sea Research Part II-*  
834 *Topical Studies in Oceanography*, 52, 2186-2205, 2005.
- 835 Alexander, V. and Chapman, T.: The role of epontic algal communities in Bering Sea ice.  
836 In: *The Eastern Bering Sea Shelf: Oceanography and Resources*, Hood, D. W. and  
837 Calder, J. A. (Eds.), University of Washington Press, Seattle, Washington, 1981.
- 838 Asahi, H., Kender, S., Ikehara, M., Sakamoto, T., Takahashi, K., Ravelo, A. C., Alvarez  
839 Zarikian, C. A., Khim, B. K., and Leng, M. J.: Orbital-scale benthic foraminiferal oxygen  
840 isotope stratigraphy at the northern Bering Sea Slope Site U1343 (IODP Expedition 323)  
841 and its Pleistocene paleoceanographic significance, *Deep Sea Research Part II: Topical*  
842 *Studies in Oceanography*, 125–126, 66-83, 2016.
- 843 Barron, J. A., Bukry, D., Dean, W. E., Addison, J. A., and Finney, B.: Paleoceanography  
844 of the Gulf of Alaska during the past 15,000 years: results from diatoms, silicoflagellates,  
845 and geochemistry, *Marine Micropaleontology*, 72, 176-195, 2009.
- 846 Bauch, H. A., Erlenkeuse, H., Helmke, J. P., and Struck, U.: A paleoclimatic evaluation  
847 of marine oxygen isotope stage 11 in the high-northern Atlantic (Nordic seas), *Global and*  
848 *Planetary Change*, 24, 27-39, 2000.
- 849 Berger, A., Crucifix, M., Hodell, D. A., Mangili, C., McManus, J. F., Otto-Bliesner, B.,  
850 Pol, K., Raynaud, D., Skinner, L. C., Tzedakis, P. C., Wolff, E. W., Yin, Q. Z., Abe-  
851 Ouchi, A., Barbante, C., Brovkin, V., Cacho, I., Capron, E., Ferretti, P., Ganopolski, A.,  
852 Grimalt, J. O., Hönisch, B., Kawamura, K., Landais, A., Margari, V., Martrat, B.,  
853 Masson-Delmotte, V., Mokeddem, Z., Parrenin, F., Prokopenko, A. A., Rashid, H.,  
854 Schulz, M., and Vazquez Riveiros, N.: “Interglacials of the last 800,000 years”, *Rev*  
855 *Geophys*, doi: 10.1002/2015RG000482, 2015. n/a-n/a, 2015.

856 Berger, A. and Loutre, M. F.: Insolation Values for the Climate of the Last 10 Million  
857 Years, *Quaternary Science Reviews*, 10, 297-317, 1991.

858 Bertrand, P., Pedersen, T. F., Martinez, P., Calvert, S., and Shimmield, G.: Sea level  
859 impact on nutrient cycling in coastal upwelling areas during deglaciation: evidence from  
860 nitrogen isotopes, *Global Biogeochemical Cycles*, 14, 341-355, 2000.

861 Bowen, D. Q.: Sea level ~400 000 years ago (MIS 11): analogue for present and future  
862 sea-level?, *Clim Past*, 6, 19-29, 2010.

863 Brigham-Grette, J., Hopkins, D. M., Ivanov, V. F., Basilyan, A. E., Benson, S. L., Heiser,  
864 P. A., and Pushkar, V. S.: Last interglacial (isotope stage 5) glacial and sea-level history  
865 of coastal Chukotka Peninsula and St. Lawrence Island, Western Beringia, *Quaternary  
866 Science Reviews*, 20, 419-436, 2001.

867 Brunelle, B. G., Sigman, D. M., Cook, M. S., Keigwin, L., Haug, G. H., Plessen, B.,  
868 Schettler, G., and Jaccard, S. L.: Evidence from diatom-bound nitrogen isotopes for  
869 subarctic Pacific stratification during the last ice age and a link to North Pacific  
870 denitrification changes, *Paleoceanography*, 22, 2007.

871 Caissie, B. E.: Diatoms as recorders of sea ice in the Bering and Chukchi seas: proxy  
872 development and application, PhD, Geosciences, University of Massachusetts Amherst,  
873 Amherst, MA, 190 pp., 2012.

874 Caissie, B. E., Brigham-Grette, J., Lawrence, K. T., Herbert, T. D., and Cook, M. S.: Last  
875 Glacial Maximum to Holocene sea surface conditions at Umnak Plateau, Bering Sea, as  
876 inferred from diatom, alkenone, and stable isotope records, *Paleoceanography*, 25,  
877 10.1029/2008pa001671, 2010.

878 Candy, I., Schreve, D. C., Sherriff, J., and Tye, G. J.: Marine Isotope Stage 11:  
879 Palaeoclimates, palaeoenvironments and its role as an analogue for the current  
880 interglacial, *Earth-Science Reviews*, 128, 18-51, 2014.

881 Chaisson, W. P., Poli, M. S., and Thunell, R. C.: Gulf Stream and Western Boundary  
882 Undercurrent variations during MIS 10 -12 at Site 1056, Blake-Bahama Outer Ridge,  
883 Marine Geology, 189, 79-105, 2002.

884 Cook, M. S., Ravelo, A. C., Mix, A., Nesbitt, I. M., and Miller, N. V.: Tracing subarctic  
885 Pacific water masses with benthic foraminiferal stable isotopes during the LGM and late  
886 Pleistocene, Deep Sea Research Part II: Topical Studies in Oceanography, 125–126, 84-  
887 95, 2016.

888 Cooper, L. W., Whitledge, T. E., Grebmeier, J. M., and Wieingartner, T.: The nutrient,  
889 salinity, and stable oxygen isotope composition of Bering and Chukchi Seas waters in  
890 and near the Bering Strait, Journal of Geophysical Research, 102, 12563-12573, 1997.

891 Cronin, T. M., Polyak, L., Reed, D., Kandiano, E. S., Marzen, R. E., and Council, E. A.:  
892 A 600-ka Arctic sea-ice record from Mendeleev Ridge based on ostracodes, Quaternary  
893 Science Reviews, 79, 157-167, 2013.

894 D'Anjou, R. M., Wei, J. H., Casteneda, I. S., Brigham-Grette, J., Petsch, S. T., and  
895 Finkelstein, D. B.: High-latitude environmental change during MIS 9 and 11:  
896 biogeochemical evidence from Lake El'gygytgyn, Far East Russia, Clim Past, 9, 567-581,  
897 2013.

898 de Vernal, A. and Hillaire-Marcel, C.: Natural variability of Greenland climate,  
899 vegetation, and ice volume during the past million years, Science, 320, 1622-1625, 2008.

900 DeBoer, A. M. and Nof, D.: The Exhaust Valve of the North Atlantic, Journal of Climate,  
901 17, 417-422, 2004.

902 Dickson, A. J., Beer, C. J., Dempsey, C., Maslin, M. A., Bendle, J. A., McClymont, E. L.,  
903 and Pancost, R. D.: Oceanic forcing of the Marine Isotope Stage 11 interglacial, Nature  
904 Geoscience, 2, 428-433, 2009.



905 Droxler, A. W., Alley, R. B., Howard, W. R., Poore, R. Z., and Burckle, L. H.: Unique  
906 and exceptionally long interglacial Marine Isotope Stage 11: window into Earth's warm  
907 future climate. In: Earth's Climate and Orbital Eccentricity: The Marine Isotope Stage 11  
908 Question, Droxler, A. W., Poore, R. Z., and Burckle, L. H. (Eds.), American Geophysical  
909 Union, Washington, DC, 2003.

910 Dutton, A., Carlson, A. E., Long, A. J., Milne, G. A., Clark, P. U., DeConto, R., Horton,  
911 B. P., Rahmstorf, S., and Raymo, M. E.: Sea-level rise due to polar ice-sheet mass loss  
912 during past warm periods, *Science*, 349, 2015.

913 Eberl, D. D.: User's Guide to RockJock--a Program for Determining Quantitative  
914 Mineralogy from Powder X-Ray Diffraction Data, US Geological Survey, Open-File  
915 Report 03-78, Boulder, CO, 2003.

916 EPICA Community Members: Eight glacial cycles from an Antarctic ice core, *Nature*,  
917 429, 623-628, 2004.

918 Flores, J. A., Gersonde, R., and Sierro, F. J.: Pleistocene fluctuations in the Agulhas  
919 Current Retroflexion based on the calcareous plankton record, *Marine*  
920 *Micropaleontology*, 37, 1-22, 1999.

921 Flores, J. A. and Sierro, F. J.: Revised technique for calculation of calcareous nannofossil  
922 accumulation rates, *Micropaleontology*, 43, 321-324, 1997.

923 Fryxell, G. A. and Hasle, G. R.: *Thalassiosira eccentrica* (Ehreb.) Cleve, *T. symmetrica*  
924 sp. nov., and some related centric diatoms, *Journal of Phycology*, 8, 297-317, 1972.

925 Glushkova, O. Y.: Geomorphological correlation of Late Pleistocene glacial complexes  
926 of Western and Eastern Beringia, *Quaternary Science Reviews*, 20, 405-417, 2001.

927 Gualtieri, L. and Brigham-Grette, J.: The age and origin of the Little Diomedede Island  
928 upland surface, *Arctic*, 54, 12-21, 2001.

- 929 Håkansson, H.: A compilation and evaluation of species in the general *Stephanodiscus*,  
930 *Cyclostephanos*, and *Cyclotella* with a new genus in the family Stephanodiscaceae,  
931 Diatom Research, 17, 1-139, 2002.
- 932 Hall, I. R., McCave, L. N., Shackleton, N. J., Weedon, G. P., and Harris, S. E.:  
933 Intensified deep Pacific inflow and ventilation in Pleistocene glacial times, Nature, 412,  
934 809-812, 2001.
- 935 Hasle, G. R. and Heimdal, B. R.: Morphology and distribution of the marine centric  
936 diatom *Thalassiosira antarctica* Comber, Journal of the Royal Microscopical Society, 88,  
937 357-369, 1968.
- 938 Hay, M. B., Dallimore, A., Thomson, R. E., Calvert, S. E., and Pienitz, R.: Siliceous  
939 microfossil record of late Holocene oceanography and climate along the west coast of  
940 Vancouver Island, British Columbia (Canada), Quaternary Research, 67, 33-49, 2007.
- 941 Hopkins, D. M.: Cenozoic History of the Bering Land Bridge, Science, 129, 1519-1528,  
942 1959.
- 943 Hopkins, D. M.: The paleogeography and climatic history of Beringia during late  
944 Cenozoic Time, Internord, 12, 121-150, 1972.
- 945 Hopkins, D. M.: Pleistocene glaciation on St. George, Pribilof Islands, Science, 1966.  
946 343-345, 1966.
- 947 Horner, R.: Sea Ice Biota, CRC Press, Inc, Boca Raton, FL, 1985.
- 948 Hu, A. X., Meehl, G. A., Otto-Bliesner, B. L., Waelbroeck, C., Han, W. Q., Loutre, M.  
949 F., Lambeck, K., Mitrovica, J. X., and Rosenbloom, N.: Influence of Bering Strait flow  
950 and North Atlantic circulation on glacial sea-level changes, Nature Geoscience, 3, 118-  
951 121, 2010.

952 Huston, M. M., Brigham-Grette, J., and Hopkins, D. M.: Paleogeographic significance of  
953 middle Pleistocene glaciomarine deposits on Baldwin Peninsula, northwestern Alaska,  
954 *Annals of Glaciology*, 14, 111-114, 1990.

955 IPCC: Climate Change 2013: The Physical Science Basis. Contribution of Working  
956 Group I to the Fifth Assessment Report of the Intergovernmental Panel on Climate  
957 Change. Stocker, T. F., Qin, D., Plattner, G.-K., Tignor, M., Allen, S. K., Boschung, J.,  
958 Nauels, A., Xia, Y., Bex, V., and Midgley, P. M. (Eds.), Cambridge University Press,  
959 Cambridge, U.K. and New York, NY, USA, 2013.

960 Iwasaki, S., Takahashi, K., Kanematsu, Y., Asahi, H., Onodera, J., and Ravelo, A. C.:  
961 Paleoproductivity and paleoceanography of the last 4.3 Myrs at IODP Expedition 323  
962 Site U1341 in the Bering Sea based on biogenic opal content, *Deep Sea Research Part II:  
963 Topical Studies in Oceanography*, 125–126, 145-154, 2016.

964 Kandiano, E. S., Bauch, H. A., Fahl, K., Helmke, J. P., Roehl, U., Perez-Folgado, M., and  
965 Cacho, I.: The meridional temperature gradient in the eastern North Atlantic during MIS  
966 11 and its link to the ocean-atmosphere system, *Palaeogeography Palaeoclimatology  
967 Palaeoecology*, 333, 24-39, 2012.

968 Kanematsu, Y., Takahashi, K., Kim, S., Asahi, H., and Khim, B.-K.: Changes in biogenic  
969 opal productivity with Milankovitch cycles during the last 1.3 Ma at IODP Expedition  
970 323 Sites U1341, U1343, and U1345 in the Bering Sea, *Quaternary International*, 310,  
971 213-220, 2013.

972 Kariya, C., Hyodo, M., Tanigawa, K., and Sato, H.: Sea-level variation during MIS 11  
973 constrained by stepwise Osaka Bay extensions and its relation with climatic evolution,  
974 *Quaternary Science Reviews*, 29, 1863-1879, 2010.

975 Kato, Y., Onodera, J., Suto, I., Teraishi, A., and Takahashi, K.: Pliocene and Pleistocene  
976 paleoceanography in the western subarctic Pacific based on diatom analyses of ODP Leg

977 145 Hole 884B and IODP Expedition 323 Holes U1341B and U1343E, Deep Sea  
978 Research Part II: Topical Studies in Oceanography, 125–126, 29-37, 2016.

979 Katsuki, K. and Takahashi, K.: Diatoms as paleoenvironmental proxies for seasonal  
980 productivity, sea-ice and surface circulation in the Bering Sea during the late Quaternary,  
981 Deep Sea Research II, 52, 2110-2130, 2005.

982 Kaufman, D. S.: Aminostratigraphy of Pliocene-Pleistocene high-sea-level deposits,  
983 Nome coastal plain and adjacent nearshore area, Alaska, Geological Society of America  
984 Bulletin, 104, 40-52, 1992.

985 Kaufman, D. S. and Brigham-Grette, J.: Aminostratigraphic correlations and  
986 paleotemperature implications, Pliocene-Pleistocene high sea-level deposits,  
987 Northwestern Alaska, Quaternary Science Reviews, 12, 21-33, 1993.

988 Kaufman, D. S., Manley, W. F., Forman, S. L., and Layer, P. W.: Pre-Late-Wisconsin  
989 glacial history, coastal Ahklun Mountains, southwestern Alaska - new amino acid,  
990 thermoluminescence, and  $^{40}\text{Ar}/^{39}\text{Ar}$  results, Quaternary Science Reviews, 20, 337-352,  
991 2001.

992 Kaufman, D. S., Walter, R. C., Brigham-Grette, J., and Hopkins, D. M.: Middle  
993 Pleistocene age of the Nome River glaciation, northwestern Alaska, Quaternary  
994 Research, 36, 277-293, 1991.

995 Keigwin, L. D., Donnelly, J. P., Cook, M. S., Driscoll, N. W., and Brigham-Grette, J.:  
996 Rapid sea-level rise and Holocene climate in the Chukchi Sea, Geology, 34, 861-864,  
997 2006.

998 Kim, S., Khim, B.-K., and Takahashi, K.: Late Pliocene to early Pleistocene (2.4–1.25  
999 Ma) paleoproductivity changes in the Bering Sea: IODP expedition 323 Hole U1343E,  
1000 Deep Sea Research Part II: Topical Studies in Oceanography, 125–126, 155-162, 2016.

- 1001 Kindler, P. and Hearty, P. J.: Elevated marine terraces from Eleuthera (Bahamas) and  
1002 Bermuda: sedimentological, petrographic, and geochronological evidence for important  
1003 deglaciation events during the middle Pleistocene, *Global and Planetary Change*, 24, 41-  
1004 58, 2000.
- 1005 Kleinen, T., Hildebrandt, S., Prange, M., Rachmayani, R., Mueller, S., Bezrukova, E.,  
1006 Brovkin, V., and Tarasov, P. E.: The climate and vegetation of Marine Isotope Stage 11-  
1007 Model results and proxy-based reconstructions at global and regional scale, *Quaternary*  
1008 *International*, 348, 247-265, 2014.
- 1009 Knudson, K. P. and Ravelo, A. C.: North Pacific Intermediate Water circulation enhanced  
1010 by the closure of the Bering Strait, *Paleoceanography*, 30, 1287-1304, 2015.
- 1011 Koizumi, I.: The Late Cenozoic diatoms of Sites 183-193, Leg 19 Deep Sea Drilling  
1012 Project, Initial Reports of the Deep Sea Drilling Project, 19, 805-855, 1973.
- 1013 Kowalik, Z.: Bering Sea Tides. In: *Dynamics of the Bering Sea*, Loughlin, T. R. and  
1014 Ohtani, K. (Eds.), University of Alaska Sea Grant, Fairbanks, AK, 1999.
- 1015 Lisiecki, L. E. and Raymo, M. E.: A Pliocene-Pleistocene stack of 57 globally distributed  
1016 benthic delta O-18 records, *Paleoceanography*, 20, 10.1029/2004PA001071, 2005.
- 1017 Liu, Z. H., Altabet, M. A., and Herbert, T. D.: Glacial-interglacial modulation of eastern  
1018 tropical North Pacific denitrification over the last 1.8-Myr, *Geophysical Research Letters*,  
1019 32, 2005.
- 1020 Lopes, C., Mix, A. C., and Abrantes, F.: Diatoms in northeast Pacific surface sediments  
1021 as paleoceanographic proxies, *Marine Micropaleontology*, 60, 45-65, 2006.
- 1022 Loutre, M. F. and Berger, A.: Marine Isotope Stage 11 as an analogue for the present  
1023 interglacial, *Global and Planetary Change*, 36, 209-217, 2003.

- 1024 Lozhkin, A. V. and Anderson, P.: Vegetation responses to interglacial warming in the  
1025 Arctic: examples from Lake El'gygytyn, Far East Russian Arctic, *Clim Past*, 9, 1211-  
1026 1219, 2013.
- 1027 Lundholm, N. and Hasle, G. R.: Are *Fragilariopsis cylindrus* and *Fragilariopsis nana*  
1028 bipolar diatoms? Morphological and molecular analyses of two sympatric species, *Nova*  
1029 *Hedwigia*, 133, 231-250, 2008.
- 1030 Lundholm, N. and Hasle, G. R.: *Fragilariopsis* (Bacillariophyceae) of the Northern  
1031 Hemisphere--morphology, taxonomy, phylogeny and distribution, with a description of  
1032 *F. pacifica* sp. nov., *Phycologia*, 49, 438-460, 2010.
- 1033 Lyle, M., Heusser, L., Herbert, T., Mix, A. C., and Barron, J.: Interglacial theme and  
1034 variations: 500 k.y. of orbital forcing and associated responses from the terrestrial and  
1035 marine biosphere, U.S. Pacific Northwest, *Geology*, 29, 1115-1118, 2001.
- 1036 Maurer, B. A. and McGill, B. J.: Chapter 5: measurement of species diversity. In:  
1037 *Biological Diversity*, Magurran, A. E. and McGill, B. J. (Eds.), Oxford University Press,  
1038 New York, 2011.
- 1039 McKay, R., Naish, T., Powell, R., Barrett, P., Scherer, R., Talarico, F., Kyle, P., Monien,  
1040 D., Kuhn, G., Jackolski, C., and Williams, T.: Pleistocene variability of Antarctic Ice  
1041 Sheet extent in the Ross Embayment, *Quaternary Science Reviews*, 34, 93-112, 2012.
- 1042 McManus, J., Oppo, D. W., Cullen, J. L., and Healey, S.: Marine Isotope Stage 11 (MIS  
1043 11): analog for Holocene and future climate. In: *Earth's Climate and Orbital Eccentricity:*  
1044 *The Marine Isotope Stage 11*, Droxler, A. W., Poore, R. Z., and Burkle, L. H. (Eds.),  
1045 *Geophysical Monograph 137*, American Geophysical Union, Washington, DC, 2003.
- 1046 McQuoid, M. R. and Hobson, L. A.: A Holocene record of diatom and silicoflagellate  
1047 microfossils in sediments of Saanich Inlet, ODP Leg 169S, *Marine Geology*, 174, 111-  
1048 123, 2001.

- 1049 Medlin, L. K. and Hasle, G. R.: Some *Nitzschia* and related diatom species from fast ice  
1050 samples in the Arctic and Antarctic, *Polar Biology*, 10, 451-479, 1990.
- 1051 Medlin, L. K. and Priddle, J.: *Polar Marine Diatoms*, British Antarctic Survey, Natural  
1052 Environment Research Council, Cambridge, 1990.
- 1053 Melles, M., Brigham-Grette, J., Minyuk, P., Nowaczyk, N. R., Wennrich, V., DeConto,  
1054 R. M., Anderson, P. M., Andreev, A. A., Coletti, A., Cook, T. L., Haltia-Hovi, E.,  
1055 Kukkonen, M., Lozhkin, A. V., Rosen, P., Tarasov, P. E., Vogel, H., and Wagner, B.: 2.8  
1056 Million years of Arctic climate change from Lake El'gygytyn, NE Russia, *Science*,  
1057 2012. 2012.
- 1058 Milker, Y., Rachmayani, R., Weinkauff, M. F. G., Prange, M., Raitzsch, M., Schulz, M.,  
1059 and Kucera, M.: Global and regional sea surface temperature trends during Marine  
1060 Isotope Stage 11, *Clim Past*, 9, 2231-2252, 2013.
- 1061 Miller, G. H., Brigham-Grette, J., Anderson, L., Bauch, H. A., Douglas, M. A., Edwards,  
1062 M. E., Elias, S. A., Finney, B. P., Funder, S., Herbert, T., Hinzman, L. D., Kaufman, D.  
1063 K., MacDonald, G. M., Robock, A., Serreze, M. C., Smol, J. P., Spielhagen, R. F., Wolfe,  
1064 A. P., and Wolff, E. W.: Temperature and precipitation history of the Arctic. In: *Past  
1065 Climate Variability and Change in the Arctic and at High Latitudes*, Research, U. S. C. C.  
1066 P. a. S. o. G. C. (Ed.), U.S. Geological Survey, Reston, VA, 2009.
- 1067 Miller, G. H. and De Vernal, A.: Will greenhouse warming lead to Northern Hemisphere  
1068 ice-sheet growth?, *Nature*, 355, 244-246, 1992.
- 1069 Muller, P. J.: C-N Ratios in Pacific Deep-Sea Sediments - Effect of Inorganic  
1070 Ammonium and Organic Nitrogen Compounds Sorbed by Clays, *Geochimica Et  
1071 Cosmochimica Acta*, 41, 765-776, 1977.
- 1072 Naish, T., Powell, R., Levy, R., Wilson, G., Scherer, R., Talarico, F., Krissek, L.,  
1073 Niessen, F., Pompilio, M., Wilson, T., Carter, L., DeConto, R., Huybers, P., McKay, R.,

- 1074 Pollard, D., Ross, J., Winter, D., Barrett, P., Browne, G., Cody, R., Cowan, E., Crampton,  
1075 J., Dunbar, G., Dunbar, N., Florindo, F., Gebhardt, C., Graham, I., Hannah, M., Hansaraj,  
1076 D., Harwood, D., Helling, D., Henrys, S., Hinnov, L., Kuhn, G., Kyle, P., Laufer, A.,  
1077 Maffioli, P., Magens, D., Mandernack, K., McIntosh, W., Millan, C., Morin, R.,  
1078 Ohneiser, C., Paulsen, T., Persico, D., Raine, I., Reed, J., Riesselman, C., Sagnotti, L.,  
1079 Schmitt, D., Sjunneskog, C., Strong, P., Taviani, M., Vogel, S., Wilch, T., and Williams,  
1080 T.: Obliquity-paced Pliocene West Antarctic ice sheet oscillations, *Nature*, 458, 322-  
1081 U384, 2009.
- 1082 Normack, W. R. and Carlson, P. R.: Giant submarine canyons: is size any clue to their  
1083 importance in the rock record? In: Geological Society of America Special Paper, Chan,  
1084 M. A. and Archer, A. W. (Eds.), Geological Society of America, Boulder, CO, 2003.
- 1085 Nürnberg, D., Wollenburg, I., Dethleff, D., Eicken, H., Kassens, H., Letzig, T., Reimnitz,  
1086 E., and Thiede, J.: Sediments in Arctic Sea-Ice - Implications for Entrainment, Transport  
1087 and Release, *Marine Geology*, 119, 185-214, 1994.
- 1088 Onodera, J. and Takahashi, K.: Diatoms and siliceous flagellates (silicoflagellates,  
1089 ebridians, and endoskeletal dinoflagellate *Actiniscus*) from the Subarctic Pacific,  
1090 *Memoirs of the Faculty of Sciences Kyushu University.*, Series D, Earth and Planetary  
1091 Sciences, 31, 105-136, 2007.
- 1092 Onodera, J., Takahashi, K., and Nagatomo, R.: Diatoms, silicoflagellates, and ebridians at  
1093 Site U1341 on the western slope of Bowers Ridge, IODP Expedition 323, *Deep Sea*  
1094 *Research Part II: Topical Studies in Oceanography*, 125–126, 8-17, 2016.
- 1095 Ortiz, J. D., Nof, D., Polyak, L., St-Onge, G., Lisé-Pronovost, A., Naidu, S., Darby, D.,  
1096 and Brachfeld, S.: The Late Quaternary Flow through the Bering Strait Has Been Forced  
1097 by the Southern Ocean Winds, *Journal of Physical Oceanography*, 42, 2014-2029, 2012.
- 1098 PAGES, P. I. W. G. o., Berger, A., Crucifix, M., Hodell, D. A., Mangili, C., McManus, J.  
1099 F., Otto-Bliesner, B., Pol, K., Raynaud, D., Skinner, L. C., Tzedakis, P. C., Wolff, E. W.,



- 1100 Yin, Q. Z., Abe-Ouchi, A., Barbante, C., Brovkin, V., Cacho, I., Capron, E., Ferretti, P.,  
1101 Ganopolski, A., Grimalt, J. O., Hoenisch, B., Kawamura, K., Landais, A., Margari, V.,  
1102 Martrat, B., Masson-Delmotte, V., Mokeddem, Z., Parrenin, F., Prokopenko, A. A.,  
1103 Rashid, H., Schulz, M., and Riveiros, N. V.: Interglacials of the last 800,000years, *Rev*  
1104 *Geophys*, 54, 162-219, 2016.
- 1105 Perdue, E. M. and Koprivnjak, J.-F.: Using the C/N ratio to estimate terrigenous inputs of  
1106 organic matter to aquatic environments, *Estuar Coast Shelf S*, 73, 65-72, 2007.
- 1107 Pol, K.: Links between MIS 11 millennial to sub-millennial climate variability and long  
1108 term trends as revealed by new high resolution EPICA Dome C deuterium data - A  
1109 comparison with the Holocene, *Clim Past*, 7, 437-450, 2011.
- 1110 Poli, M. S., Meyers, P. A., and Thunell, R. C.: The western North Atlantic record of MIS  
1111 13 to 10: Changes in primary productivity, organic carbon accumulation and benthic  
1112 foraminiferal assemblages in sediments from the Blake Outer Ridge (ODP Site 1058),  
1113 *Palaeogeography, Palaeoclimatology, Palaeoecology*, 295, 89-101, 2010.
- 1114 Pollard, D. and DeConto, R. M.: Modelling West Antarctic ice sheet growth and collapse  
1115 through the past five million years, *Nature*, 458, 329-U389, 2009.
- 1116 Prokopenko, A. A., Bezrukova, E. V., Khursevich, G. K., Solotchina, E. P., Kuzmin, M.  
1117 I., and Tarasov, P. E.: Climate in continental interior Asia during the longest interglacial  
1118 of the past 500 000 years: the new MIS 11 records from Lake Baikal, SE Siberia, *Clim*  
1119 *Past*, 6, 31-48, 2010.
- 1120 Pushkar, V. S., Roof, S. R., Cherepanova, M. V., Hopkins, D. M., and Brigham-Grette,  
1121 J.: Paleogeographic and paleoclimatic significance of diatoms from Middle Pleistocene  
1122 marine and glaciomarine deposits on Baldwin Peninsula, northwestern Alaska,  
1123 *Palaeogeography, Palaeoclimatology, Palaeoecology*, 152, 67-85, 1999.

- 1124 Raymo, M. E. and Mitrovica, J. X.: Collapse of polar ice sheets during the stage 11  
1125 interglacial, *Nature*, 483, 453-456, 2012.
- 1126 Raymo, M. E., Mitrovica, J. X., O'Leary, M. J., DeConto, R. M., and Hearty, P. J.:  
1127 Departures from eustasy in Pliocene sea-level records, *Nature Geoscience*, 4, 328-332,  
1128 2011.
- 1129 Raynaud, D., Barnola, J. M., Souchez, R., Lorrain, R., Petit, J. R., Duval, P., and  
1130 Lipenkoy, V. Y.: The record for Marine Isotopic Stage 11, *Nature*, 436, 39-40, 2005.
- 1131 Reimnitz, E., McCormick, M., Bischof, J., and Darby, D. A.: Comparing sea-ice  
1132 sediment load with Beaufort Sea shelf deposits: is entrainment selective?, *Journal of*  
1133 *Sedimentary Research*, 68, 777-787, 1998.
- 1134 Reyes, A. V., Carlson, A. E., Beard, B. L., Hatfield, R. G., Stoner, J. S., Winsor, K.,  
1135 Welke, B., and Ullman, D. J.: South Greenland ice-sheet collapse during Marine Isotope  
1136 Stage 11, *Nature*, 510, 525-+, 2014.
- 1137 Rohling, E. J., Braun, K., Grant, K., Kucera, M., Roberts, A. P., Siddall, M., and  
1138 Trommer, G.: Comparison between Holocene and Marine Isotope Stage-11 sea-level  
1139 histories, *Earth and Planetary Science Letters*, 291, 97-105, 2010.
- 1140 Rohling, E. J., Foster, G. L., Grant, K. M., Marino, G., Roberts, A. P., Tamisiea, M. E.,  
1141 and Williams, F.: Sea-level and deep-sea-temperature variability over the past 5.3 million  
1142 years (vol 508, pg 477, 2014), *Nature*, 510, 432-432, 2014.
- 1143 Saito, K. and Taniguchi, A.: Phytoplankton communities in the Bering Sea and adjacent  
1144 seas II: spring and summer communities in seasonally ice-covered areas, *Astarte*, 11, 27-  
1145 35, 1978.
- 1146 Sancetta, C. A.: Distribution of diatom species in surface sediments of the Bering and  
1147 Okhotsk seas, *Micropaleontology*, 28, 221-257, 1982.

- 1148 Sancetta, C. A.: Oceanographic and ecologic significance of diatoms in surface sediments  
1149 of the Bering and Okhotsk seas, *Deep Sea Research*, 28A, 789-817, 1981.
- 1150 Sancetta, C. A.: Three species of *Coscinodiscus* Ehrenberg from North Pacific sediments  
1151 examined in the light and scanning electron microscopes, *Micropaleontology*, 33, 230-  
1152 241, 1987.
- 1153 Sancetta, C. A. and Robinson, S. W.: Diatom evidence on Wisconsin and Holocene  
1154 events in the Bering Sea, *Quaternary Research*, 20, 232-245, 1983.
- 1155 Sancetta, C. A. and Silvestri, S. M.: Pliocene-Pleistocene evolution of the North Pacific  
1156 ocean-atmosphere system, interpreted from fossil diatoms, *Paleoceanography*, 1, 163-  
1157 180, 1986.
- 1158 Schandelmeier, L. and Alexander, V.: An analysis of the influence of ice on spring  
1159 phytoplankton population structure in the southeast Bering Sea, *Limnology and*  
1160 *Oceanography*, 26, 935-943, 1981.
- 1161 Scherer, R. P.: A new method for the determination of absolute abundance of diatoms  
1162 and other silt-sized sedimentary particles, *Journal of Paleolimnology*, 12, 171-179, 1994.
- 1163 Scherer, R. P., Aldahan, A., Tulaczyk, S., Possnert, G., Engelhardt, H., and Kamb, B.:  
1164 Pleistocene collapse of the West Antarctic Ice Sheet, *Science*, 281, 82-85, 1998.
- 1165 Schlung, S. A., Ravelo, A. C., Aiello, I. W., Andreasen, D. H., Cook, M. S., Drake, M.,  
1166 Dyez, K. A., Guilderson, T. P., LaRiviere, J. P., Stroynowski, Z., and Takahashi, K.:  
1167 Millennial-scale climate change and intermediate water circulation in the Bering Sea  
1168 from 90 ka: A high-resolution record from IODP Site U1340, *Paleoceanography*, 28,  
1169 2013.
- 1170 Schrader, H. J. and Gersonde, R.: Diatoms and silicoflagellates. In: *Micropaleontological*  
1171 *counting methods and techniques - an exercise on an eight metres section of the Lower*

- 1172 Pliocene of Capo Rossello, Sicily, Zachariasse, W. J., Riedel, W. R., Sanfilippo, A.,  
1173 Schmidt, R. R., Brolsma, M. J., Schrader, H. J., Gersonde, R., Drooger, M. M., and  
1174 Broekman, J. A. (Eds.), Utrecht Micropaleontological Bulletin, Netherlands, 1978.
- 1175 Schubert, C. J. and Calvert, S. E.: Nitrogen and carbon isotopic composition of marine  
1176 and terrestrial organic matter in Arctic Ocean sediments: implications for nutrient  
1177 utilization and organic matter composition, *Deep Sea Research I*, 48, 789-810, 2001.
- 1178 Schumacher, J. D. and Stabeno, P. J.: Continental shelf of the Bering Sea. In: *The sea*,  
1179 Robinson, A. R. and Brink, K. H. (Eds.), John Wiley and Sons, New York, 1998.
- 1180 Shiga, K. and Koizumi, I.: Latest Quaternary oceanographic changes in the Okhotsk Sea  
1181 based on diatom records, *Marine Micropaleontology*, 38, 91-117, 2000.
- 1182 Sigman, D., Altabet, M., Francois, R., McCorkle, D., and Gaillard, J.-F.: The isotopic  
1183 composition of diatom-bound nitrogen in Southern Ocean sediments, *Paleoceanography*,  
1184 14, 118-134, 1999.
- 1185 Smol, J. P.: The paleolimnologist's Rosetta Stone: calibrating indicators to environmental  
1186 variables using surface-sediment training sets. In: *Pollution of lakes and rivers: a  
1187 paleoenvironmental perspective*, Smol, J. P. (Ed.), Key issues in environmental change,  
1188 Oxford University Press, New York, 2002.
- 1189 Springer, A. M., McRoy, C. P., and Flint, M. V.: The Bering Sea green belt: shelf edge  
1190 processes and ecosystem production, *Fisheries Oceanography*, 5, 205-223, 1996.
- 1191 St. John, K.: Cenozoic ice-rafting history of the central Arctic Ocean: Terrigenous sands  
1192 on the Lomonosov Ridge, *Paleoceanography*, 23, 10.1029/2007pa001483, 2008.
- 1193 Stabeno, P. J., Schumacher, J. D., and Ohtani, K.: The physical oceanography of the  
1194 Bering Sea. In: *Dynamics of the Bering Sea: a summary of physical, chemical, and*

1195 biological characteristics, and a synopsis of research on the Bering Sea, Loughlin, T. R.  
1196 and Ohtani, K. (Eds.), University of Alaska Sea Grant, Fairbanks, AK, 1999.

1197 Stroynowski, Z., Ravelo, A. C., and Andreasen, D.: A Pliocene to recent history of the  
1198 Bering Sea at Site U1340A, IODP Expedition 323, *Paleoceanography*, 30, 1641-1656,  
1199 2015.

1200 Syvertsen, E. E.: Resting Spore Formation in Clonal Cultures of *Thalassiosira antarctica*  
1201 Comber, *T. nordenskioeldii* Cleve and *Detonula confervacea* (Cleve) Gran, *Nova*  
1202 *Hedwigia*, 64, 41-63, 1979.

1203 Takahashi, K., Ravelo, A. C., Alvarez Zarikian, C. A., and Scientists, E.: Proceedings of  
1204 the Integrated Ocean Drilling Program. Tokyo, 2011.

1205 Tarasov, P. E., Nakagawa, T., Demske, D., Österle, H., Igarashi, Y., Kitagawa, J.,  
1206 Mokhova, L., Bazarova, V., Okuda, M., Gotanda, K., Miyoshi, N., Fujiki, T., Takemura,  
1207 K., Yonenobu, H., and Fleck, A.: Progress in the reconstruction of Quaternary climate  
1208 dynamics in the Northwest Pacific: A new modern analogue reference dataset and its  
1209 application to the 430-kyr pollen record from Lake Biwa, *Earth-Science Reviews*, 108,  
1210 64-79, 2011.

1211 Teitler, L., Florindo, F., Warnke, D. A., Filippelli, G. M., Kupp, G., and Taylor, B.:  
1212 Antarctic Ice Sheet response to a long warm interval across Marine Isotope Stage 31: A  
1213 cross-latitudinal study of iceberg-rafted debris, *Earth and Planetary Science Letters*, 409,  
1214 109-119, 2015.

1215 Teraishi, A., Suto, I., Onodera, J., and Takahashi, K.: Diatom, silicoflagellate and  
1216 ebridian biostratigraphy and paleoceanography in IODP 323 Hole U1343E at the Bering  
1217 slope site, *Deep Sea Research Part II: Topical Studies in Oceanography*, 125–126, 18-28,  
1218 2016.

- 1219 Ternois, Y., Kawamura, K., Keigwin, L., Ohkouchi, N., and Nakatsuka, T.: A biomarker  
1220 approach for assessing marine and terrigenous inputs to the sediments of Sea of Okhotsk  
1221 for the last 27,000 years, *Geochimica et Cosmochimica Acta*, 65, 791-802, 2001.
- 1222 Tomas, C. R.: *Identifying marine diatoms and dinoflagellates*, Academic Press, Inc.  
1223 Harcourt Brace and Co., Boston, U.S.A., 1996.
- 1224 Tzedakis, P. C.: The MIS 11 – MIS 1 analogy, southern European vegetation,  
1225 atmospheric methane and the “early anthropogenic hypothesis”, *Clim Past*, 6, 131-144,  
1226 2010.
- 1227 van Hengstum, P. J., Scott, D. B., and Javaux, E. J.: Foraminifera in elevated Bermudian  
1228 caves provide further evidence for +21m eustatic sea level during Marine Isotope Stage  
1229 11, *Quaternary Science Reviews*, 28, 1850-1860, 2009.
- 1230 Voelker, A. H. L., Rodrigues, T., Billups, K., Oppo, D., McManus, J., Stein, R., Hefter,  
1231 J., and Grimalt, J. O.: Variations in mid-latitude North Atlantic surface water properties  
1232 during the mid-Brunhes (MIS 9–14) and their implications for the thermohaline  
1233 circulation, *Clim Past*, 6, 531-552, 2010.
- 1234 Vogel, H., Meyer-Jacob, C., Melles, M., Brigham-Grette, J., Andreev, A. A., Wennrich,  
1235 V., Tarasov, P. E., and Rosen, P.: Detailed insight into Arctic climatic variability during  
1236 MIS 11c at Lake El'gygytgyn, NE Russia, *Clim Past*, 9, 1467-1479, 2013.
- 1237 von Quillfeldt, C. H.: Identification of some easily confused common diatom species in  
1238 Arctic spring blooms, *Botanica Marina*, 44, 375-389, 2001.
- 1239 von Quillfeldt, C. H., Ambrose, W. G. J., and Clough, L. M.: High number of diatom  
1240 species in first-year ice from the Chukchi Sea, *Polar Biology*, 26, 806-818, 2003.
- 1241 Witkowski, A., Lange-Bertalot, H., and Metzeltin, D.: *Diatom Flora of Marine Coasts I*,  
1242 A.R.G. Gantner Verlag K.G., Ruggell, Liechtenstein, 2000.

- 1243 Young, J. R., Geisen, M., Cros, L., Keleijne, A., Sprengel, C., Probert, I., and  
1244 Østengaard, J.: A guide to extant coccolithophore taxonomy, *Journal of Nannoplankton*  
1245 *Research, Special Issue*, 1, 1-125, 2003.  
1246

1247 **Table 1:** Age-Depth Tie Points Used in the Age Model for U1345

1248

<b>Depth (m CCSF-A)</b>	<b>Age (ka)</b>	<b>Date Type</b>
98.6	337	Foraminifera {Cook, 2016}
115.3	374	Foraminifera {Cook, 2016}
123.2	398.5	Magnetic Susceptibility Correlation
130.6	424	Foraminifera {Cook, 2016}
148.7	478	Foraminifera {Cook, 2016}

1249

1250 **Table 2:** Depths and Ages of major climate intervals referred to in the text

<b>Interval</b>	<b>Depth begin (m CCSF-A)</b>	<b>Depth end (m CCSF-A)</b>	<b>Begin (ka)</b>	<b>End (ka)</b>
Late MIS 11/10	121.80	110.57	394	364
Beringian Glacial Initiation	124.94	121.80	405	394
Peak MIS 11	130.16	121.80	423	394
Termination V	131.09	130.16	425	423
MIS 12	133.10	131.09	431	425

1251



1252 Table 3: Bering Sea diatom species grouped by environmental niche. In cases where a species appears in more than one niche, the  
 1253 grouping used in this study is highlighted in bold.

<i>Modern Seasonal Succession</i>			
<b>Epontic</b>	<b>Marginal Ice Zone (MIZ)</b>	<b>Both Epontic and MIZ</b>	<b>Summer Bloom</b>
<i>Navicula transitrans</i>	<b><i>Bacterosira bathyomphala</i></b>	<i>Actinocyclus curvatus</i>	<b><i>Coscinodiscus</i> spp.</b>
<i>Nitzschia frigida</i>	<i>Chaetoceros furcellatus</i>	<b><i>Fossula arctica</i></b>	<b><i>Leptocylindrus</i> sp.</b>
	<i>Chaetoceros socialis</i>	<b><i>Fragilariopsis cylindrus</i></b>	<b><i>Rhizosolenia</i> spp.</b>
	<i>Leptocylindrus</i> sp.	<b><i>Fragilariopsis oceanica</i></b>	
	<i>Odontella aurita</i>	<b><i>Navicula pelagica</i></b>	
	<i>Paralia sulcata</i>	<b>Naviculoid pennates</b>	
	<b><i>Porosira glacialis</i></b>	<b><i>Nitzschia</i> spp.</b>	
	<b><i>Staurosirella</i> cf. <i>pinnata</i></b>	<b><i>Pinnularia quadratarea</i></b>	
	<i>Thalassionema nitzschioides</i>	<b><i>Thalassiosira antarctica</i></b>	
	<b><i>Thalassiosira angulata</i></b>	<b><i>Thalassiosira gravida</i></b>	
	<b><i>Thalassiosira baltica</i></b>		
	<b><i>Thalassiosira decipiens</i></b>		
	<b><i>Thalassiosira hyalina</i></b>		
	<b><i>Thalassiosira hyperborea</i></b>		
	<b><i>Thalassiosira nordenskiöldii</i></b>		
	<i>Thalassiosira pacifica</i>		

1254 Continued on next page

Table 3 continued

<i>Water Mass Tracers</i>				<i>Shelf to Basin Transport</i>	
<b>Dicothermal</b>	<b>High Productivity</b>	<b>Alaska Stream</b>	<b>Warmer Water</b>	<b>Neritic</b>	<b>Fresh Water</b>
<i>Actinocyclus curvatulus</i>	<i>Chaetoceros</i> spp.	<i>Neodenticula seminae</i>	<i>Azpeitia tabularis</i>	<i>Actinoptychus senarius</i>	<i>Lindavia</i> cf. <i>ocellata</i>
<i>Shionodiscus trifultus</i>	<i>Odontella aurita</i>		<i>Stellarimia stellaris</i>	<i>Amphora</i> sp.	<i>Lindavia stylorum</i>
	<i>Thalassionema nitzschioides</i>		<i>Thalassionema nitzschioides</i>	<i>Lindavia stylorum</i>	<i>Staurosirella</i> cf. <i>pinnata</i>
	<i>Thalassiosira pacifica</i>		<i>Thalassiosira eccentrica</i>	<i>Delphineis</i> spp.	<i>Lindavia radiosa</i>
	<i>Thalassiosira</i> spp. small		<i>Thalassiosira oestrupii</i>	<i>Dentonula confervacea</i>	
	<i>Thalassiothrix longissima</i>		<i>Thalassiosira symmetrica</i>	<i>Diploneis smithii</i>	
				Naviculoid pennates	
				<i>Odontella aurita</i>	
				<i>Paralia sulcata</i>	
				<i>Rhaphoneis ampiceros</i>	
				<i>Stephanopyxis turris</i>	
				<i>Thalassiosira angulata</i>	
				<i>Thalassiosira decipiens</i>	
				<i>Thalassiosira eccentrica</i>	

1256 **Table 4:** Distribution of Laminated Intervals during MIS 11. Note that the depth and age  
 1257 of laminated intervals encompasses all holes drilled, but the median duration is  
 1258 calculated using each of the holes that it is present in.

Lamination	Type	Depth (mbsf)	Age (ka)	Median Duration (kyrs)	Found in Holes
MIS 11.5	II	112.02-111.47	367.23-366.00	0.51	CDE
MIS 11.4	II	113.14-112.94	369.72-369.26	0.34	CD
MIS 11.3	II	114.28-113.95	372.25-371.52	0.73	D
MIS 11.2	II	115.59-114.69	374.75-373.17	1.23	ACE
MIS 11.1	II	121.84-121.18	394.12-392.09	1.10	CE
Termination V	I	130.23-126.51	423.28-410.44	12.04	ACDE

1259 **Table 5:** Summary Statistics for X-Ray Diffraction  
 1260

	Mean	Standard	Minimum	Maximum
Full pattern degree of	0.257	0.014	0.242	0.282
<b>Mineral</b>	(wt.	(wt. %)	(wt. %)	(wt. %)
<i>Non-clays</i>				
Quartz	14	2	9	16
Kspar	1	1	0	2
Plag	9	2	5	12
Calcite	Tr	Tr	0	1
Aragonite	2	1	0	3
Dolomite	2	1	1	3
Siderite	1	1	0	2
Amphibole	4	1	3	5
Pyroxene	1	1	0	2
Pyrite	1	0	0	1
Magnetite	Tr	Tr	0	1
Hematite	Tr	Tr	0	1
Goethite	Tr	Tr	0	0
Maghemite	Tr	Tr	0	1
Titanite	1	1	0	3
Tephra	21	5	16	35
Zircon	Tr	Tr	0	0
<i>Total Non-clays</i>	57	2	54	63
<i>Clays</i>				
Kaolinite	0	0	0	0
Smectite	0	0	0	0
Illite	8	3	2	11
Biotite	2	1	0	3
Chlorite	33	3	29	38
Muscovite	Tr	1	0	2
<i>Total Clays</i>	43	2	37	46
<b>Total</b>	100			

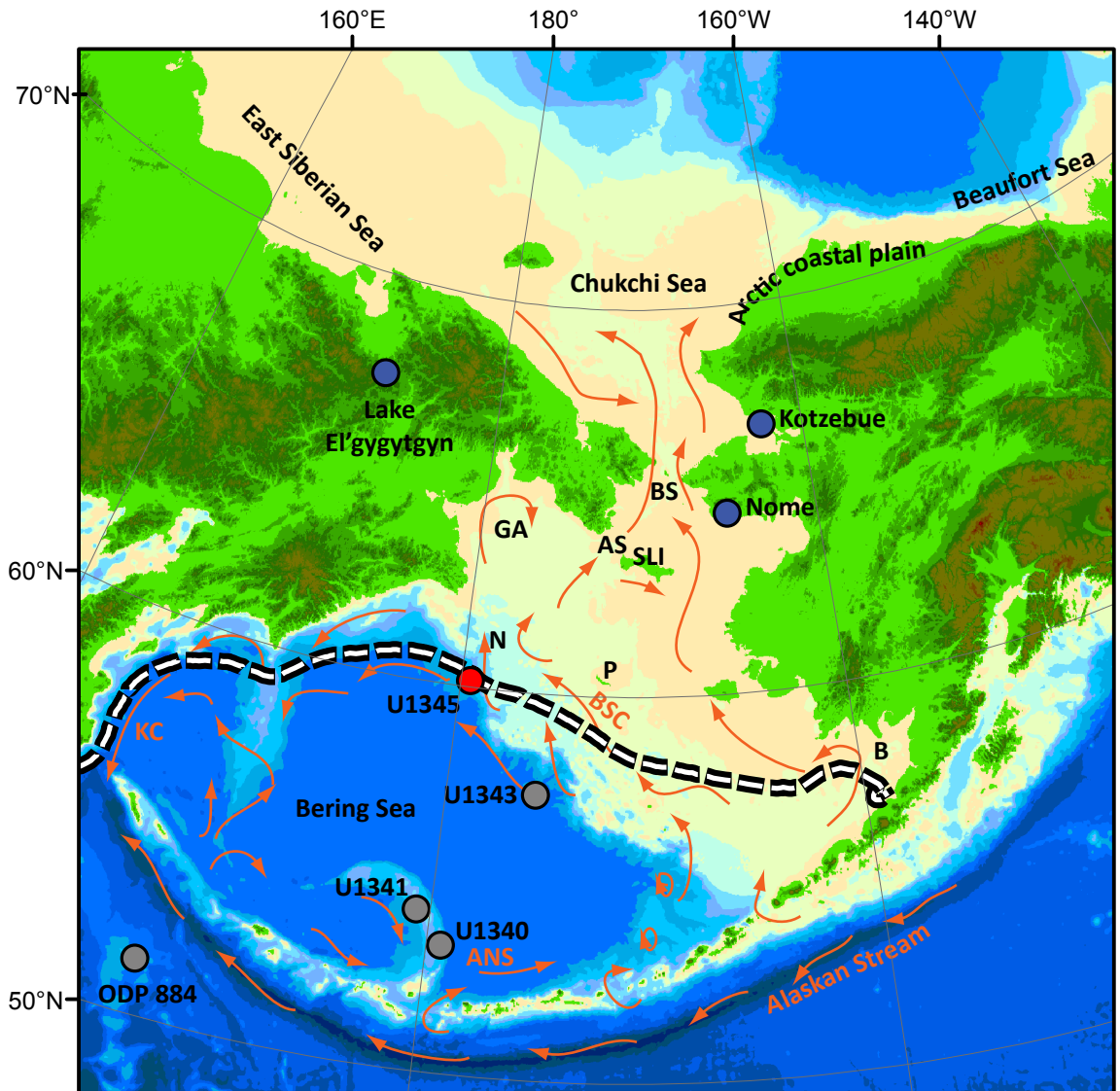


**Figure 1.** Map of Beringia with locations of cores mentioned in the text (U1345 (red dot), and U1340, U1341, U1343, and ODP Site 884 (grey dots)). Locations of place names from the text are labeled: Aleutian North Slope Current (ANS), Anadyr Strait (AS), Bristol Bay (B), Bering Strait (BS), Bering Slope Current (BSC), Gulf of Anadyr (GA), Kamchatka Current (KC), Navarin Canyon (N), Pribilof Islands (P), St. Lawrence Island (SLI). The white and black dashed line is the maximum extent of sea ice (median over the period 1979-2013) (Cavaliere et al., 1996). Currents are in orange and are modified from Stabeno (1999). Base map is modified from Manley (2002).

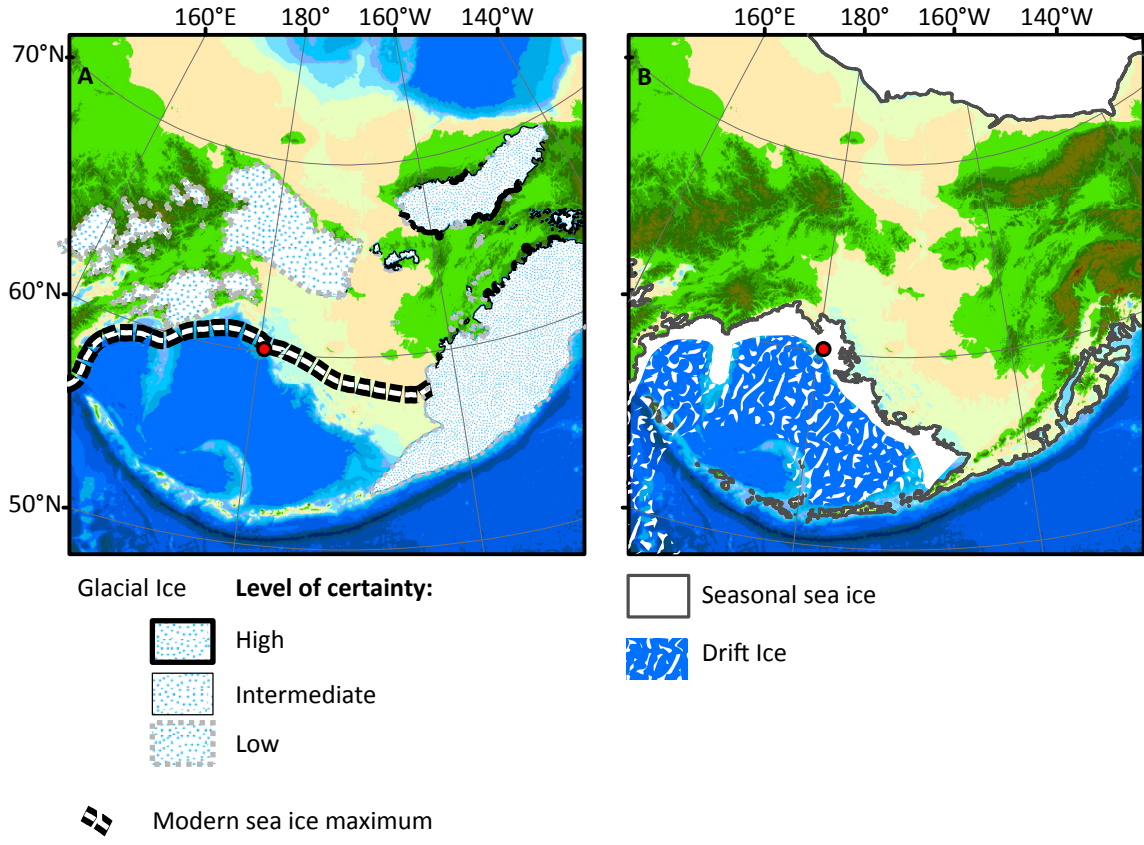


**Figure 2.** Maximum glacial and sea ice extents in Beringia. A. depicts the maximum glacial ice in Beringia as inferred from terminal and lateral moraines. This is not intended to show the maximum extent during a particular glaciation, but rather the maximum possible extent of glacial ice. These moraines are likely from several different major glaciations. The level of certainty is indicated by the thickness of the line at the moraine. The white and black dashed line is the maximum extent of sea ice (median over period 1979-2013) (Cavaliere et al., 1996). B. depicts the approximate pattern of sea ice during glacial stages (Katsuki and Takahashi, 2005). The dark grey contour is -140 m asl, the approximate sea level during MIS 12 (Rohling et al., 2010). Base map is modified from Manley (2002).

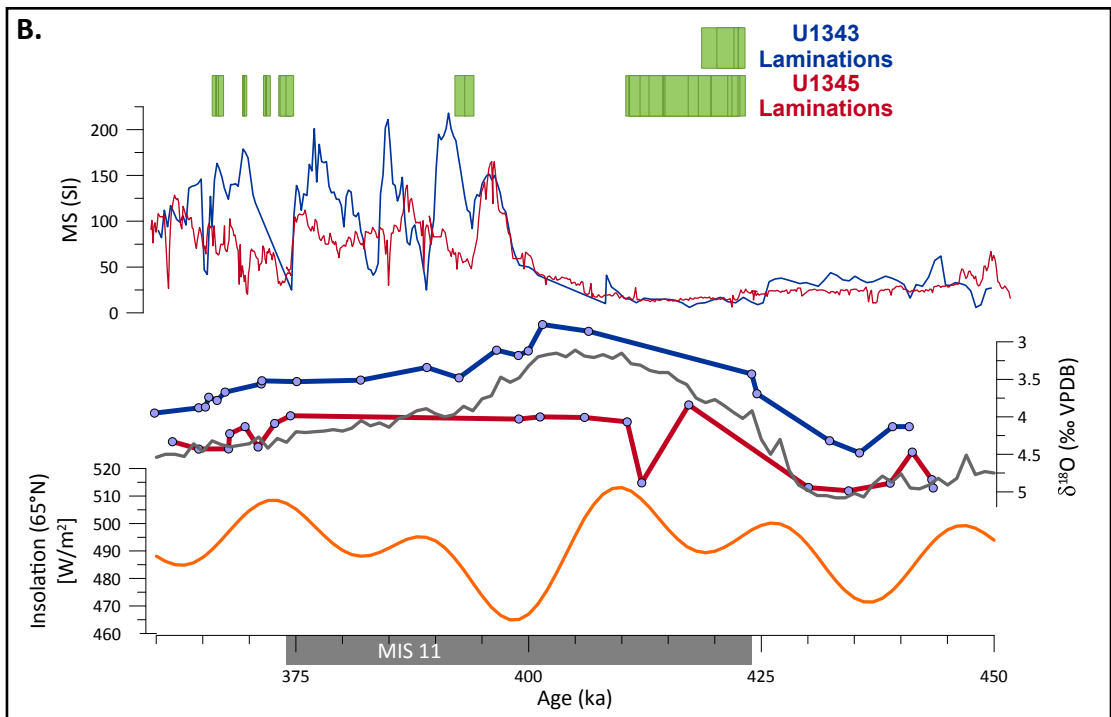
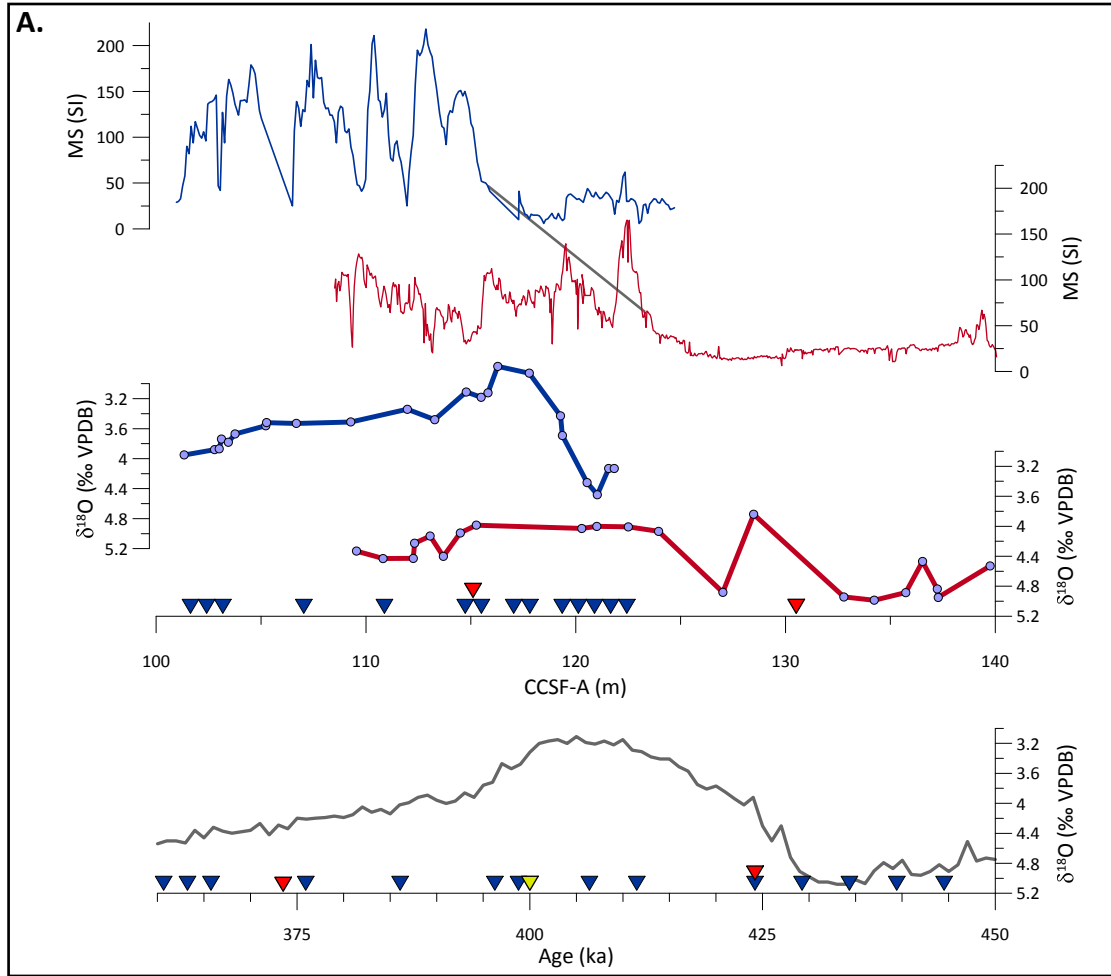


**Figure 3.**

1261 **Figure 3A.** Age model plotted by depth. Blue plots depict data from Site U1343, red  
1262 plots are from U1345. Magnetic susceptibility and benthic foraminiferal  $\delta^{18}\text{O}$  are plotted  
1263 by depth for each Site in the top half of the figure. The grey line joining the magnetic  
1264 susceptibility plots indicates the tie point that was added in this study. Inverted triangles  
1265 indicate locations of tie points (red: U1345, blue: U1343, grey: magnetic susceptibility)  
1266 between Bering Sea  $\delta^{18}\text{O}$  (Cook et al., 2016; Asahi et al., 2016) and the global marine  
1267 stack (Lisiecki and Raymo, 2005), which is plotted in grey. **B:** Age model plotted by age.  
1268 Magnetic susceptibility and  $\delta^{18}\text{O}$  are shown with the global marine  $\delta^{18}\text{O}$  stack (grey) and  
1269 insolation at  $65^\circ\text{ N}$  (orange). Green bars indicate laminated intervals in U1343 and  
1270 U1345.

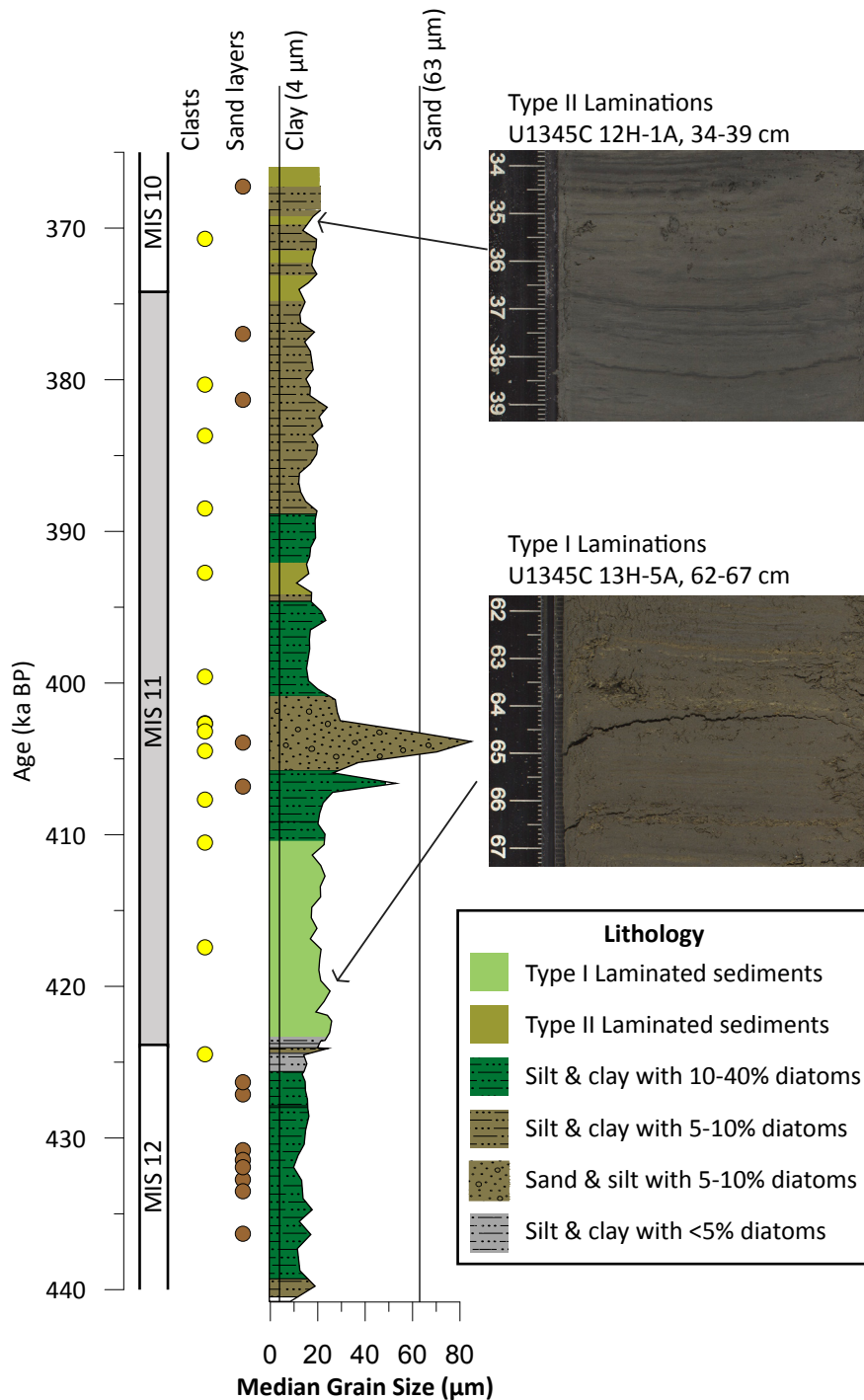


**Figure 4.** Lithostratigraphic column for U1345A. Marine Isotope Stage 11 is depicted as a grey bar. Ice rafted debris (yellow dots) and sand layers (maroon dots) are a compilation of these features in all four holes at U1345. The width of the lithologic column varies according to median grain size. Vertical lines indicate the cut off for clay and sand sized particles. Silt lies between the two lines. Colors depict varying amounts of diatoms relative to terrigenous grains in the sediment. Type I Laminations are depicted as pale green bars and Type II laminations are depicted as olive green bars. An example of each of the lamination types is shown in the images to the right.



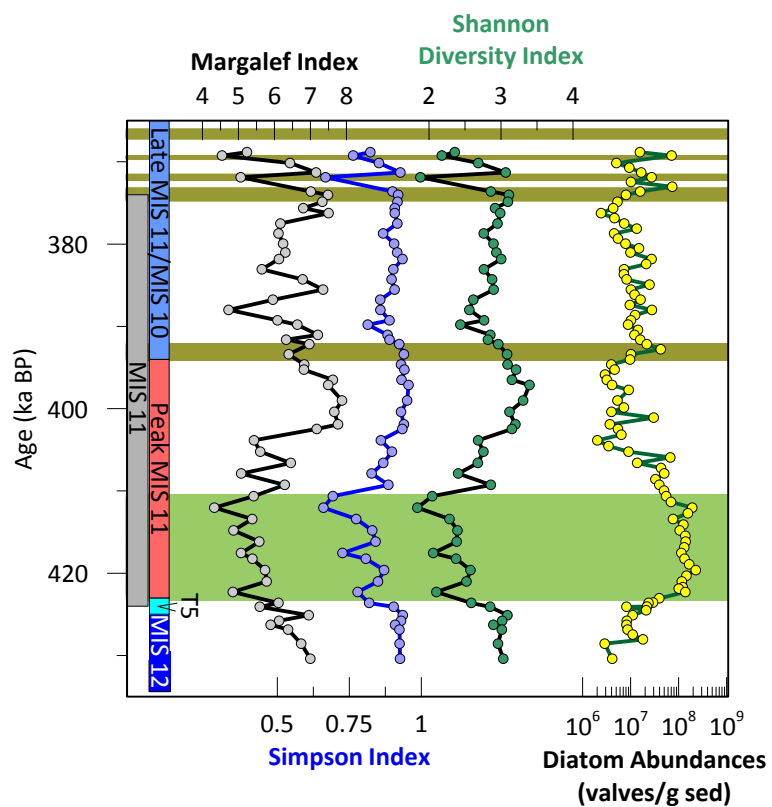


**Figure 5.** The Margalef, Simpson, and Shannon diversity indices plotted with diatom abundances. Type I Laminations are depicted as pale green bars and Type II laminations are depicted as olive green bars. Colored vertical bars refer to the zones mentioned in the text.

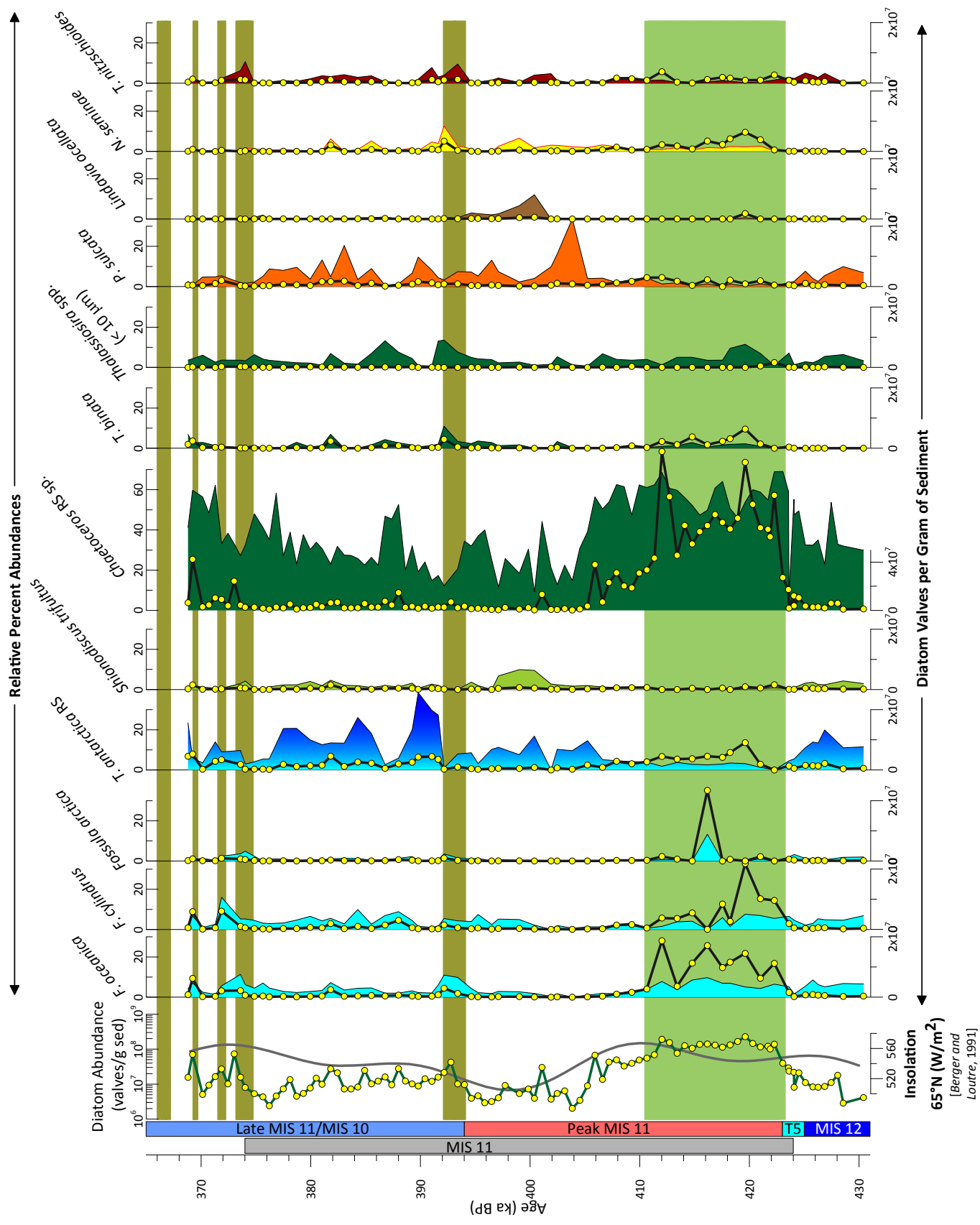


Figure 6.

1271 **Figure 6.** Absolute and relative percent abundances of all diatoms that occur in  
1272 abundances greater than 10% of any assemblage. Colored vertical bars refer to the zones  
1273 mentioned in the text. Line plots depict absolute abundance and area plots depict relative  
1274 percent abundance. Species are color coded according to the niche that they are grouped  
1275 into: marginal ice zone (light blue), both ice types (dark blue to light blue), dicothermal  
1276 (light green), high productivity (green), neritic (orange), freshwater (brown), North  
1277 Pacific (yellow), and warm water (red). Insolation 65° N (light grey line) is also shown.  
1278 Type I Laminations are depicted as pale green bars and Type II laminations are depicted  
1279 as olive green bars.

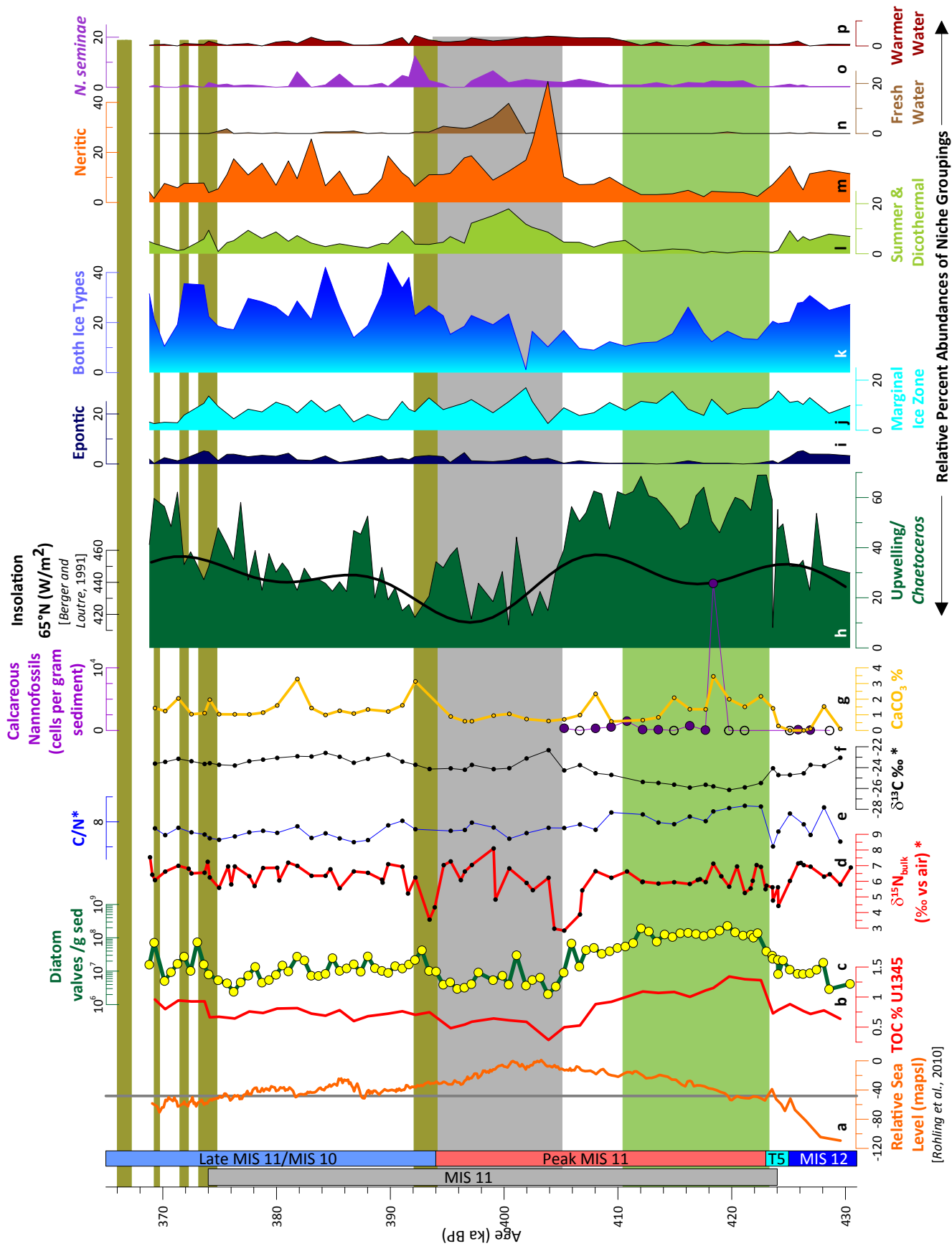
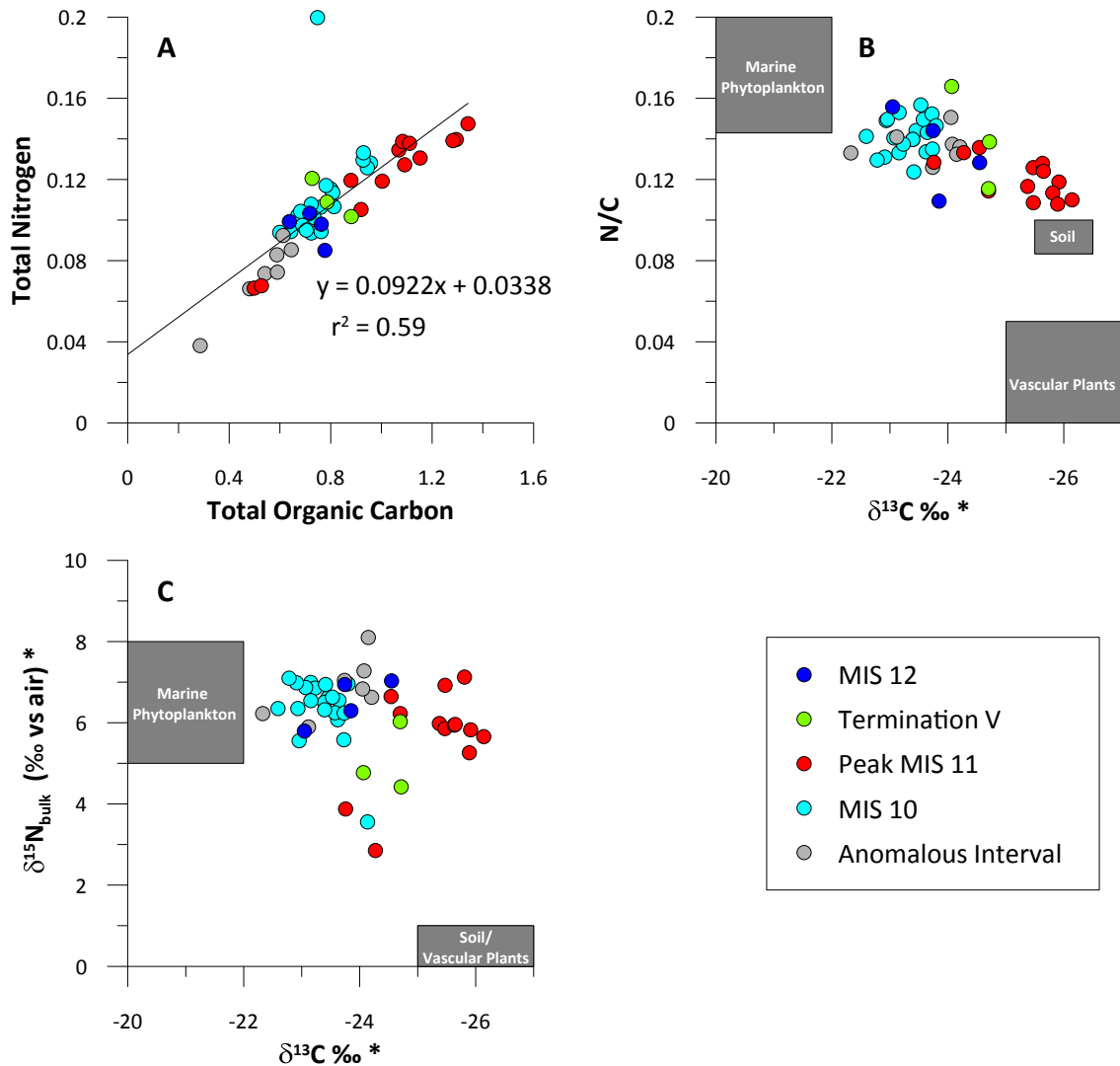
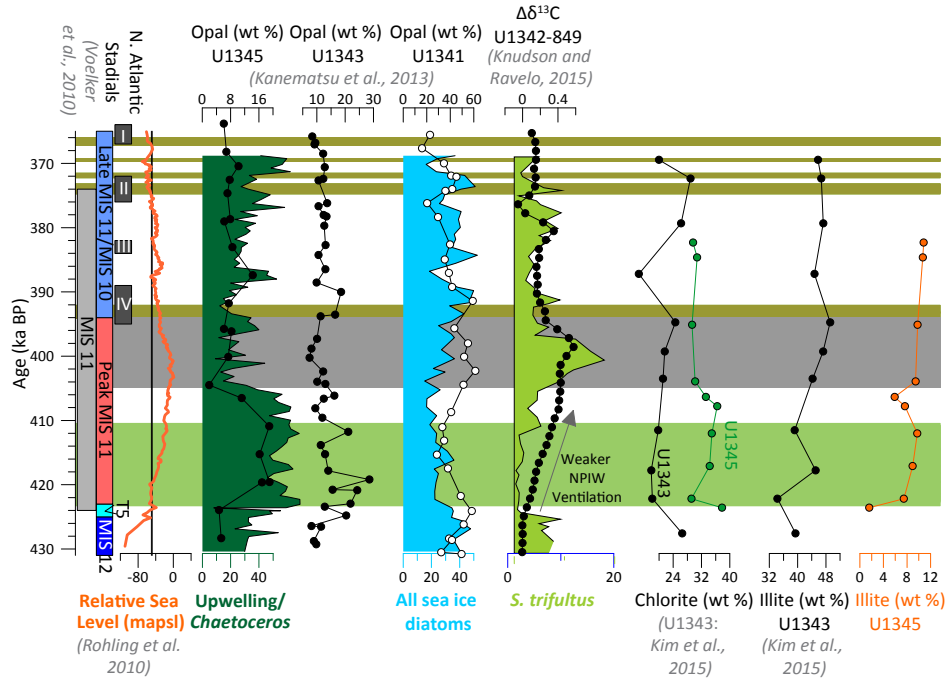


Figure 7.

1280 **Figure 7.** Summary of geochemistry and biological proxies. The grey vertical bar depicts  
1281 the duration of MIS 11 and colored vertical bars refer to the zones mentioned in the text.  
1282 **A.** Global eustatic sea level (orange) is plotted for reference (Rohling et al., 2010). The  
1283 sill depth of Bering Strait (-50 m apsl) is shown as a vertical grey line. Total organic  
1284 carbon (**B.** red) is plotted with the total diatom abundance (**C.** green line, yellow dots).  
1285 Geochemical data is plotted as  $\delta^{15}\text{N}$  (**D.** red), C/N (**E.** blue),  $\delta^{13}\text{C}$  (**F.** black), and %  
1286  $\text{CaCO}_3$  (**G.** yellow). Biological proxies include absolute abundance of calcareous  
1287 nannofossils (**G.** purple). Open circles indicate barren samples; closed circles indicate  
1288 samples that had calcareous nannofossils present. Relative percent abundances of diatoms  
1289 are grouped by environmental niche. *Chaetoceros* RS are green (**H.**), epontic species are  
1290 navy blue (**I.**), marginal ice zone species are light blue (**J.**), species that fall under both  
1291 ice categories are shaded with a gradational blue (**K.**), summer and dicothermal species  
1292 are light green (**L.**), neritic species are orange (**M.**), fresh water species are brown (**N.**),  
1293 *N. seminae* is purple (**O.**), and warmer water species are maroon (**P.**). Insolation at 65° N  
1294 (black) is overlain on *Chaetoceros* RS relative percent abundances. Type I Laminations  
1295 are depicted as pale green bars and Type II laminations are depicted as olive green bars.  
1296 A grey bar indicates the Beringian glacial advance.



**Figure 8.** Crossplots of **A.** total nitrogen vs. total organic carbon, **B.**  $\text{N}/\text{C}_{\text{rg}}$  vs.  $\delta^{13}\text{C}$ , and **C.**  $\delta^{15}\text{N}$  vs.  $\delta^{13}\text{C}$ . For each panel, the range of composition of each organic matter source is plotted in a grey box: marine phytoplankton (C/N: 5-7 (Redfield, 1963; Meyers, 1994);  $\delta^{13}\text{C}$ : -19‰ to -22‰ (Schubert and Calvert, 2001);  $\delta^{15}\text{N}$ : 5‰ to 8‰ (Walinsky et al., 2009)); Soil (C/N: 10-12,  $\delta^{13}\text{C}$ : -25.5‰ to -26.5‰,  $\delta^{15}\text{N}$ : 0‰ to 1‰ (Walinsky et al., 2009)); C3 vascular plants (C/N: > 20 (Redfield, 1963; Meyers, 1994);  $\delta^{13}\text{C}$ : -25‰ to -27‰ (Schubert and Calvert, 2001);  $\delta^{15}\text{N}$ : 0‰ to 1‰ (Walinsky et al., 2009)).



**Figure 9.** Comparison of Site U1345 with other Bering Sea (U1340, U1341, U1343) and global sites. The grey vertical bar depicts the duration of MIS 11, colored vertical bars refer to the zones mentioned in the text, and dark grey bars show the timing of North Atlantic stadials (I-IV) (Voelker et al., 2010). Global eustatic sea level (orange) is plotted for reference (Rohling et al., 2010). The sill depth of Bering Strait (-50 m apsl) is shown as a vertical grey line. Weight % opal from Sites U1345, U1343, and U1341 (Kanematsu et al., 2013) is plotted with *Chaetoceros* RS relative percent abundances, and relative percent abundances of all sea ice diatoms. The difference in benthic foraminiferal  $\delta^{13}\text{C}$  between the Bowers Ridge (U1342) and the North Pacific (ODP 849), a proxy for North Pacific Intermediate Water ventilation, is plotted with relative percent abundances of *Shionodiscus trifultus*, an indicator of highly stratified water. Note that ventilation increases to the left. The weight percent of the clay minerals, chlorite and illite are plotted for Sites U1343 (Kim et al., 2015) and U1345 (this study). Type I Laminations are depicted as pale green bars and Type II laminations are depicted as olive green bars. A grey bar indicates the “anomalous interval.”

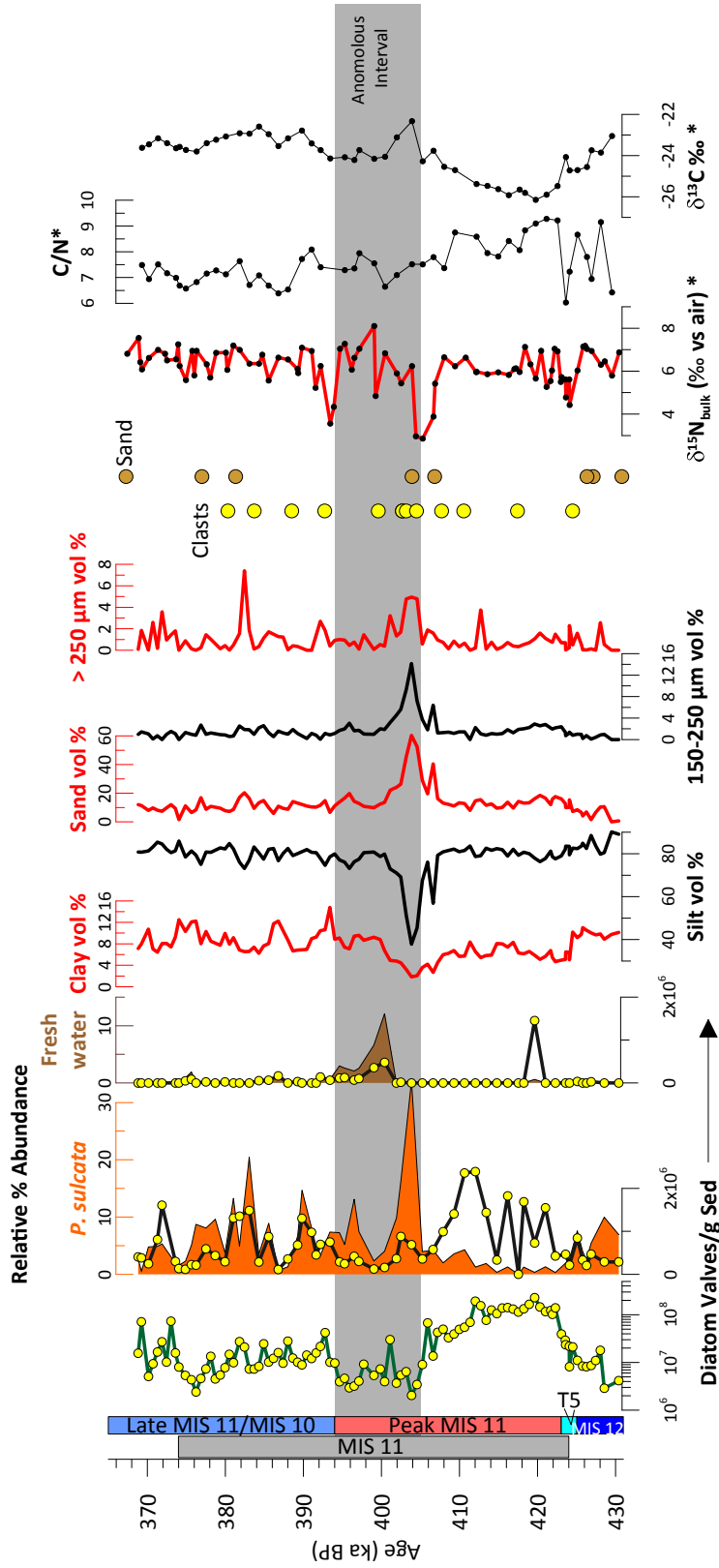


**Figure 10.** Proxy indicators of shelf to basin transport. The grey vertical bar depicts the duration of MIS 11, colored vertical bars refer to the zones mentioned in the text. Total diatom absolute abundances are plotted next to absolute (line plots) and relative percent abundance of *P. sulcata* (orange area plot) and fresh water species (brown area plot). High-resolution grain size includes % clay, sand, and greater than 250  $\mu\text{m}$  (red lines) and % silt and 150-250  $\mu\text{m}$  (black lines). High-resolution indicate isolated clasts (IRD), maroon circles indicate sand layers for all holes at U1345. Geochemical data is plotted as  $\delta^{15}\text{N}$  (red),  $\text{C/N}$  (black), and  $\delta^{13}\text{C}$  (black). The grey bar spans 405-394 ka, the so-called, “anomalous interval.”